Chemistry: Student Scholarship & Creative Works

Chemistry & Biochemistry

Spring 2016

Preparation and Characterization of Osmium Complexes For Use in Luminescent Metal Organic Frameworks

Libby A. Hemler
Elizabethtown College, hemlerl@etown.edu

Recommended Citation

Preparation and Characterization of Osmium Complexes
For Use in Luminescent Metal Organic Frameworks

By

Libby A. Hemler

A Thesis Submitted
in Partial Fulfillment of
the Requirements of Honors in the Discipline and
the Elizabethtown College Honors Program

Department of Chemistry
Elizabethtown College
May 6, 2016

Elizabethtown College
Department of Chemistry & Biochemistry

The Thesis submitted by

Libby A. Hemler

under the title

"Preparation and Characterization of Osmium Complexes For Use in Luminescent Metal-Organic Frameworks"

has been read and undersigned. It is hereby recommended for acceptance
in partial fulfillment of the graduation requirements for
Department Honors in Chemistry & Biochemistry

_____   _____
(Signed) Thomas E. Hagan, Jr.   (Date)

_____   _____
(Signed) Gary G. Hoffman   (Date)

_____   _____
(Signed) Kristi A. Kneas   (Date)
Research Advisor

_____   _____
(Signed) James A. MacKay   (Date)

_____   _____
(Signed) Jeffrey A. Rood   (Date)

Recommendation accepted by the Chair of the Department of Chemistry & Biochemistry,
Elizabethtown College:

                                                                _____
                                                                (Signed) Kristi A. Kneas

                                                                _____
                                                                (Date)

Abstract

Metal-organic frameworks (MOFs) consist of metal ion centers complexed with organic linkers to form an extended three-dimensional, porous structure. These materials have broad applications in separation, small molecule storage, catalysis, and, increasingly, in analytical sensing. In particular, luminescence-based sensing should be possible by preparation of luminescent metal-organic frameworks (LMOFs) whose photophysical properties vary upon changing host-guest interactions. In the current work, LMOFs are prepared from zinc(II) ions and luminescent transition metal complexes: $[Os(bpy)_2(dcbpy)]Cl_2$, $[Os(phen)_2(dcphen)]Cl_2$, and $[Os(CO)_2Cl_2(dcbpy)]$. Systematic alterations were made to the ligands of the luminescent transition metal complexes in order to discern the impact on the photoluminescence of the complexes and the LMOFs. The excitation and emission spectra are reported for the transition metal complex in solution and solid state and compared to those obtained for the LMOF. Insights gained will be applied in the development of sensors for analyte-specific sensors of environmental or clinical interest.

Table of Contents

List of Figures

List of Appendices

INTRODUCTION

Optical Sensing

Chemical sensors provide a straightforward and cost-effective method of determining the presence and concentration of various analytes and are applicable for use in the medical, pharmaceutical, environmental, and food industries.[1] In particular, *optical* sensors provide additional advantages in these fields. Optical methods have the advantage of being a more portable method of detection for various analytes instead of using bulky instruments.[1] Recently, an optical sensor was used in the field to determine the amount of phytochemical compounds in cabbage. Researchers were able to nondestructively determine the optimum amount of flavonoids and chlorophyll which were synthesized in the crops based on different growing conditions.[1] In another example, an optical sensor was developed to detect small amounts of chloroform in solutions, both aqueous and nonaqueous. This thin film sensor was placed into the solution, and upon interaction with chloroform, it produced a color change that was able to be analyzed spectroscopically in order to determine the concentration of chloroform in that particular solution remotely.[2]

Optical analyses, such as pH sensing, humidity sensing, quantification of analytes, and many other applications, have arisen from the wide applicability of these methods and their usefulness.[3] Much of the current interest in developing new methods of sensing stemmed originally from the previous use of radioactive components, as they can be harmful to both the human population and the environment.[4] In addition, researchers are interested in decreasing both the cost and the time associated with many of the proposed

alternative methods while increasing the sensitivity and selectivity provided using these optical methods. Given these desirable figures of merit, fluorescence in optical sensing is often preferable to absorbance, since fluorimeters measure emission against a dark background as opposed to the brightness of a reference beam and thus have excellent sensitivity. In addition, the detection limits of fluorescence measurements are much smaller than the detection limits for absorbance, on the order of ppb compared to ppm. Furthermore, the amount of fluorescent molecules is more limited than the number which absorb light, giving fluorescence measurements the advantage of being more selective than absorbance measurements. Additionally, a comparatively small amount of fluorescent material is required to obtain appreciable signal.[4]

Use of luminescent transition metal complexes (TMCs) in solution is one example of a common luminescence-based sensing scheme; their desirable photophysical properties made tunable by changing their ligands make them particularly useful. Luminescent complexes, such as $[Ru(bpy)_3]^{2+}$ and $[Os(bpy)_3]^{2+}$, have low interference, good separation between their emission and excitation spectral peaks, and relatively long excited state lifetimes, which is the average time it takes the molecule to relax back down to the ground state.[5] In addition, the luminescence intensity and sometimes the maximum emission wavelength of the TMC complex change due to variations in the environment of the complex, thus providing another sensing strategy. Luminescent metal complexes that exhibit changes in their intensity, excited state lifetimes, and emission maxima in response to analytes have been used to determined oxygen, chloride, and CO_2 concentrations, as well as to determine the pH of solutions.[5] However, a large

disadvantage of this sensing method is the non-uniform emission and quenching response of the TMC that results upon integration of the transition metal complex into the necessary support matrix. This results in poor sensor film-film reproducibility and necessitates more complex calibrations in order to obtain useful data.[6]

A different type of fluorescence sensing mechanism makes use of Förster resonance energy transfer (FRET). Typically, FRET is utilized when a fluorescent analyte of interest emits at a wavelength which is close to the wavelength of excitation of a second, reporter molecule. This allows for selectivity when it comes to particular analytes as well as providing the fluorescence properties required. In order to shift the measured emission to longer wavelengths, the sensor molecule, which is within the Förster distance of the analyte of interest, is added to the solution. This permits an energy transfer between the donor (analyte) and acceptor (secondary reporter) molecules in order to increase the ease of determining emissions from the initial analyte molecule.[4] FRET analyses have been proposed as a means of indicating the presence of Botulinum neurotoxin, which is recognized as a potential public health problem. In order to measure the emission of the neurotoxin, quantum dots were introduced into the system for the FRET transfer to occur between semiconductor quantum dot donor and the chromophore conjugated acceptor neurotoxin, which allowed the testing to be performed accurately in the field. [7] However, maintaining the correct Förster distance required for this transfer to occur has been noted to be a disadvantage of this method and thus may not allow accurate quantification of the analyte studied.

The problem of too great a distance between the FRET donor and acceptor molecules could be addressed with a nanostructure containing a capture agent coating the surface. In this approach, instead of placing the optical sensor into the sample, a small amount of the sample is directly applied to the surface of a membrane. If the applied sample is complimentary to the capture agent, it will adhere to the surface. This method is further enhanced using a sandwich assay method, which layers an antigen, the sample, and the complimentary antibody. The antigen on the surface attracts the sample when the sample is delivered onto the surface. Washing the surface rids the structure of all other components of the sample mixture. An antibody, which typically contains a fluorescent tag, is then applied allowing the sample to be visualized. However, this method requires that the target analyte be specific to the antigen and antibody combination used thus limiting the approach to select analytes.[8]

Luminescence-Based Sensors Exploiting Environment-Sensitive TMCs

Considering the limitations of these different types of fluorescence sensing mechanisms, it is evident that there remains a need for a method with broad versatility for application to a large number of analytes to be detected, with good sensitivity and selectivity. As such, previous work leading up to the current project was directed at studies of the potential of a new class of luminescence-based sensors which make use of smart hydrogels supports. An environment-sensitive fluorophore was incorporated into a hydrogel film in order to determine relative humidity. The hydrogel film swells and contracts based on the relative humidity in its surrounding system and the emissions of

4

the luminophore inside the hydrogel change after the swelling of the film. The swelling and contracting of the "smart" hydrogel was in response to a change in the environment due to the introduction of an analyte. By incorporating an environmentally-sensitive luminophore, such as dapoxyl sulfonic acid (DSA), into the hydrogel matrix, the film exhibits a shift to longer emission wavelengths when its solvent is more polar. The combination of both changes allowed for emissions responding to both the polarity of the solvent and the relative humidity in the system. Advantages of this method are the simplicity of the construction of this type of sensor and the breadth of applications for this methodology, based on the "smart" hydrogels' environment sensitivity. Furthermore, these hydrogels exhibit sensitivity for gas phase measurements and could exhibit selectivity due to the smart hydrogel support matrix, while the luminophore can be a reporter molecule for many different analytes. However, it became apparent that a major disadvantage of this type of sensor stemmed from the ability of the luminophore to leach out of the hydrogel.[3a] The successes made by the research group in this particular project have catalyzed a new project involving luminescent metal-organic frameworks as a support matrix instead of the hydrogel film.

Similarly to the previous hydrogel work, the new work focuses on the integration of luminophores to a metal organic framework. It has been proposed that luminescent transition metal complexes will be able to achieve a similar environment responsivity as organic luminophores such as DSA. When designed appropriately, these complexes are sensitive to the local environment and may exhibit different emission intensities or wavelengths in those varying environments. Due to the issue of leaching encountered

previously, it has been proposed to integrate the metal complex into a metal organic

framework, as the luminophore would be embedded into the hydrogel support matrix

itself, unable to leave the framework of the sensor.

Metal organic frameworks are composed of a metal complex and organic linkers

that create an extended crystal lattice-type structure. Figure 1 shows how a MOF is

formed when combining the metal ion and organic linker. In the current work, the

osmium transition metal complexes will take the place of the organic linkers.

Metal
Ion

Organic Linker

Extended MOF Structure
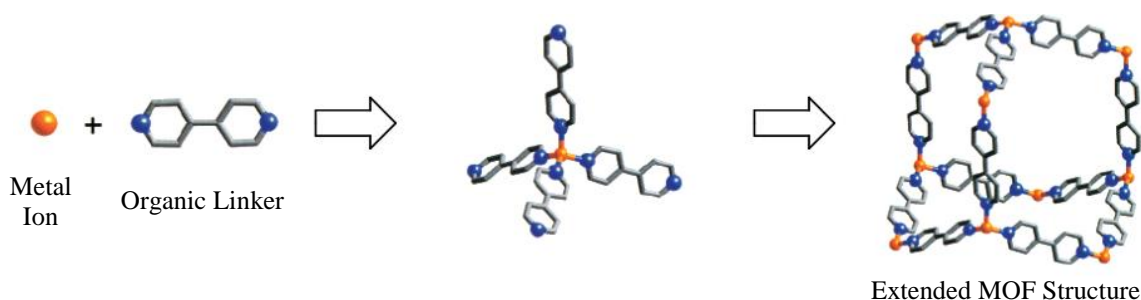
Figure 1. Depiction of the composition of a single unit MOF crystal

Based on the choice of organic linkers, the size of the pores in the metal organic

framework structure can be altered, allowing for selective uptake of particular analytes.[9]

Additionally, the selectivity of the MOF can be changed by varying the groups inside the

pores to be selective to one particular analyte. Furthermore, the inside of the MOF pore

can be functionalized in order to specifically target the covalent interactions between

MOF functional groups and analytes of interest.[10] This specificity for select analytes is

what is being capitalized on this work through the creation of different transition metal

complexes which will be able to interact with certain analytes and not others. In addition,

the rigidity of the MOF can also decrease the movement of the metal complex, therefore

changing the complex's emissions. Utilizing the MOF as a sensor will rely on changes in the emission intensity and emission wavelengths to determine the concentration and presence of the analytes being detected.

While work with MOFs is still relatively new in the field of chemistry, they have become of significant importance due to their wide applicability, including uses as drug delivery vehicles, for gas transport and storage, and in optical sensing.[11] In using MOFs for drug delivery, the organic linkers allow for the variation in the size of the pores to maximize the amount of drug taken up, and the metal centers are adjusted in order to allow for specific release of the drug from the MOF. Additionally, bioMOFs have been proposed, which incorporate a specific biomolecule in the framework in order to further control the release of drugs present in its pores. MOFs can also be used for the storage of different gases, such as NO in the body and H_2 for fuel cells. The most relevant application of MOFs to this work is their use as sensors for oxygen, glucose, and other biomolecules. This involves the incorporation of a luminescent substance in the structure of the MOF that interacts with these molecules and creates a change in the emissions of LMOFs themselves.[11]

Measurements of emissions can be monitored in a few different ways: a change in emission wavelength and a change in emission intensity being the most common. For example, a pCO_2 sensor utilizing diketo-pyrrolo-pyrrole pigments embedded in a film matrix provided researchers with a change in maximum emission wavelength when the sensors was exposed to changes in pH as a result of the presence of CO2. When in acidic conditions, the sensor resulted in a blue shift in the emission wavelength of about 50nm.

This allowed for the determination of pCO_2 in a solution based on the maximum emission wavelength.[12] Additionally, optical sensors can rely on changes in emission intensity as their guiding principle. A study utilizing quantum dots measured their luminescence quenching in the presence of hemin, an Fe(III)-protoporphyrin complex. Quenching causes a decrease in emission intensity when measuring at the same wavelength due to the presence of analyte, hemin. This allows for a calibration curve to be obtained and the concentration of hemin in an unknown sample can be determined using the resulting standard curve.[13]

Principles of Photoluminescence

At the core of the functionality of these luminescent metal-organic frameworks as reporter molecules is the phenomenon of photoluminescence, in which a substance emits electromagnetic radiation after being excited by electromagnetic radiation. This emission can ensue in one of two ways, fluorescence or phosphorescence. A way of illustrating these occurrences is through use of a Jablonski energy level diagram, as seen in Figure 1. Typically, a molecule rests at lowest energy in the ground state, S_0, in which all electrons are paired. Additional electronic states in which the molecule can exist have increased quantized energies, such as the singlet states S_1 and S_2. To these singlet excited states, one of the paired electrons can be excited, and it retains its initial spin. Each electronic state also contains different quantized vibrational states, as seen by the lighter lines above the bolded line in Figure 2. There are also triplet excited states an electron can occupy, such as T_1, which also have multiple vibrational states. In a triplet state, the excited

electron undergoes a spin flip, resulting in the formerly paired electrons becoming

unpaired.[14]
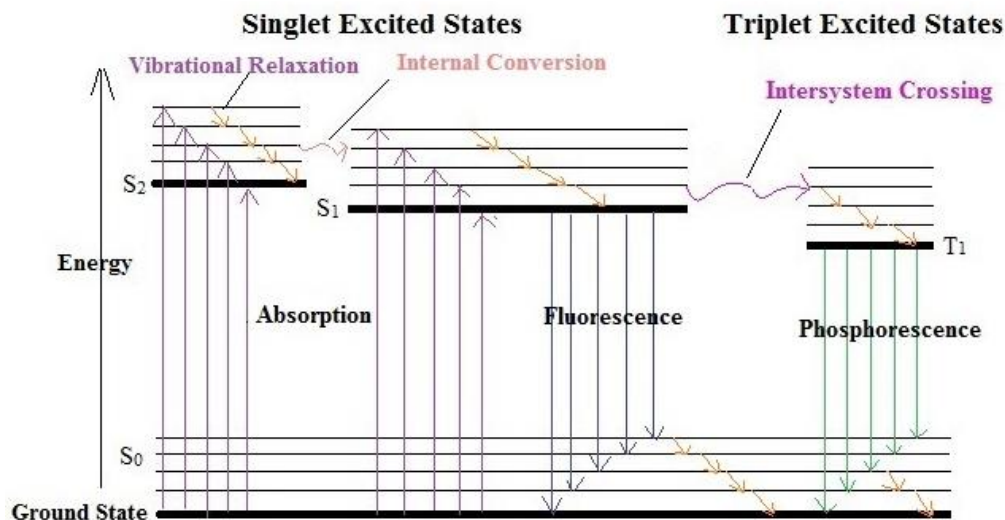
Figure 2. Jablonski diagram of the partial energy-level diagram for a photoluminescent system.

In photoluminescent compounds, energy of particular wavelengths added to a

molecule can excite them to higher energy electronic states, provided the energy is equal

to the gap between the energy states. This process is called absorption and can cause a

change in vibrational states as well. However, a molecule will typically relax back down

to the lowest energy vibrational state, as illustrated by the bold lines on Figure 1, in what

is known as vibrational relaxation. This process occurs quite rapidly, on the order of

10^{-12} s, and is the result of molecules colliding with one another in solution, which allows

them to give off energy and relax to the lowest energy level. From this level, the

molecule can also relax down to lower energy singlet states with the same spin as the

previous state, which is referred to as internal conversion. Since molecules are most

stable in their ground state energy level, from either excited singlet state, the molecule will relax back down to the ground state. This is a radiative process, meaning that light is emitted, and because no spin flip is required, it is called fluorescence. Fluorescence lifetimes, or the average time the molecule stays in an excited energy state, are on the order of 10^{-5} ns, indicating a relatively rapid process.[14]

A molecule in an excited singlet state can also undergo intersystem crossing from a singlet excited state to enter a triplet excited state of lower energy, as seen from the movement from the S_1 state to the T_1 state in Figure 1, through a spin conversion. From this state, the molecule can relax back down to the ground state, undergoing a spin flip in the process, and produce phosphorescence. Phosphorescence is a longer process than fluorescence, on the order of microseconds to a few seconds, as the transitions between triplet and singlet states are typically forbidden. However, excited states of heavy atoms, such as osmium, have character of both triplet and singlet character due to an increase in intersystem crossing, leading to emissions with properties of both phosphorescence and fluorescence.[14] In regards to the current work, the emission given off by the osmium transition metal-complexes is referred to as luminescence as it exhibits characteristics of both fluorescence and phosphorescence.[15]

Design of Luminescence TMCs and LMOFs

Many of the metals (e.g. Ru, Os, Re) used in the synthesis of luminescent transition metal complexes (TMCs) have partially filled d-orbitals. As seen in Figure 2, the more easily the metal ion is oxidized, the larger the energy gap between the d and d*

orbitals of the metal center when comparing complexes with the same ligands, as a stronger bond is formed between the transition metal and the attached ligands. This allows the metal-to-ligand charge transfer (MLCT) to occur more readily in osmium complexes as the energy required to overcome this energy gap is less than the energy required for the same transition in Ru^{2+} complexes, indicating one advantage of using osmium in the TMCs. As the energy required for MLCT in osmium metal complexes is lower than the energy needed for ruthenium complexes, they emit at longer wavelengths than ruthenium complexes.[15]
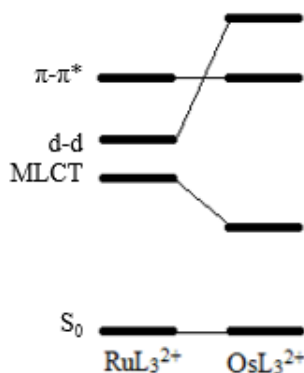
Figure 3. Energy level diagram comparing transitions in Ru and Os TMCs[15]

Also of importance is the choice of ligand attached to the metal center, as it can increase the gap between the d to d* transition of the metal complex to ensure that the MLCT transition is lowest in energy, making it the most predominant. Ensuring that this is the lowest energy transition is crucial, as the d to d* transition is forbidden. In this particular research the ligand choice has focused on aromatic ligands, such as the α-diimines 2,2'-bipyridine (bpy), 4,4'-dicarboxy-2,2'-bipyridine (dcbpy), 1,10-phenanthroline (phen), and 4,7-dicarboxy-1,10-phenanthroline (dcphen), as well as

carbonyls. Additionally, these aromatic ligands have low radiative lifetimes, which give off a higher luminescence, increasing the intensity of the MLCT, which is the transition exploited in this work. On one of the proposed complexes, carbonyls are added instead of aromatic ligands. Adding carbonyls to the complexes increases the energy required to make the d to d* transition, as they are electron withdrawing groups and pull electron density needed to make this transition away from the metal center. Additionally, the carbonyl groups shift emissions to shorter wavelengths and destabilize the excited states of the complexes, which increases the energy required to be introduced into the system.[15]

For the current work, osmium complexes utilizing the electronic properties of the ligands discussed previously were synthesized. A benefit of the osmium complexes used in this research is that they can be incorporated into thermally stable sensors that give consistent light emissions when characterized at many different temperatures due to the large separation between the states in the osmium complex.[16] In particular, osmium metal complexes have been synthesized, keeping constant the addition of a dicarboxylated organic ligand, but varying the other ligands on the central osmium ion. The dicarboxylated ligands attached were carboxylated bipyridine and carboxylated phenanthroline to promote the MLCT transition, and the other ligands were either two carbonyls and two chlorides or two ligands which are the same as the dicarboxylated ligand but without the carboxylic acid groups. As the TMCs are taking the place of the organic linkers in the MOFs, a carboxyl group is required to link together the metal ions, which is the reasoning behind including the dicarboxylated ligands on the TMCs.

Additionally, the changes in the ligands will impact the formation of the pores inside the LMOF, as larger ligands will take up more space inside the pore.

In particular, the complexes [Os(bpy)₂(dcbpy)]Cl₂, [Os(phen)₂(dcphen)]Cl₂, [Os(CO)₂Cl₂(dcbpy)], and [Os(CO)₂Cl₂(dcphen)] have been proposed to be studied, where bpy is 2,2'-bipyridine, dcbpy is 2,2'-bipyridine-4,4'-dicarboxylic acid, phen is 1,10-phenanthroline, and dcphen is 1,10-phenanthroline-4,7-dicarboxylic acid. The compound [Os(bpy)₂(dcbpy)] Cl₂ has been reported at least seven times previously in the literature, but the compound [Os(phen)₂(dcphen)]Cl₂ has not been previously reported.[17] Additionally, the compound [Os(CO)₂Cl₂(dcbpy)] has been reported only once previously in the literature, and the compound [Os(CO)₂Cl₂(dcphen)] has not been previously reported.[18] Therefore, this work and future work will represent the first comprehensive analysis of this family of compounds with regards to their luminescence properties.
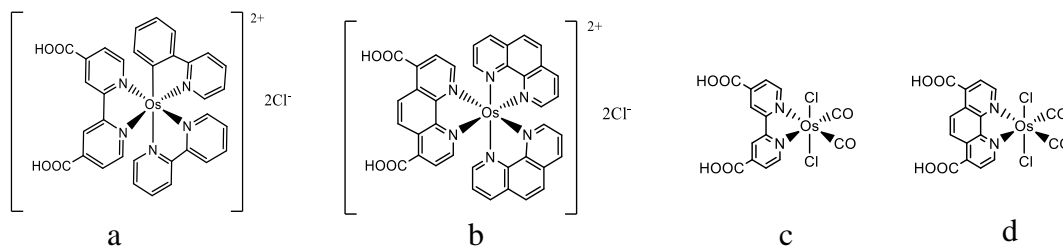
Figure 4. Structures of [Os(bpy)₂(dcbpy)]Cl₂ (a), [Os(phen)₂(dcphen)]Cl₂ (b), [Os(CO)₂Cl₂(dcbpy)] (c), and [Os(CO)₂Cl₂(dcphen)] (d)

Osmium transition metal complexes such as those utilized in the current work have also been proposed for a variety of different purposes in addition to their use as in optical sensors. Similar complexes have been analyzed for their electrochemical properties, indicating the potential use of these complexes for electrochemical sensing.[19]

Additionally, osmium arene complexes were determined to be cytotoxic to human cancer cells when at small concentrations. Previous to this cancer research, similar studies were performed on ruthenium complexes, but as these complexes caused cytotoxicity of cells, the focus was shifted to osmium as the metal of choice.[20] Thus, there is significant value in the addition of these novel osmium complexes and an understanding of their photophysical properties to those published previously in the literature.

Once these complexes are synthesized, they are incorporated into a luminescent metal-organic framework (LMOF). As indicated previously, an LMOF is a porous material, which will allow for the entrance of analytes. As the analyte interacts with the crystalline structure, it should result in a change in the luminescence properties of the LMOF, ideally inducing a measurable change in the emission intensity and/or wavelength. Evidence to suggest the likelihood of this change could be found in a previous study of the photophysics of luminescent metal complexes in rigid supports, such as in glycerol. It has been indicated that the rigidity of the environment in which the molecule is located along with changes in the environment can cause changes in the emission wavelengths and intensities of metal complexes.[21] The changes in emission properties based on the rigidity of the complexes' environment can be exploited by systematic changes in the ligands.

In addition to calibrating emission intensity and maximum emission wavelength changes in response to analyte, another property of these transition metal complexes of great interest because of potential for analyte detection is their fluorescence anisotropy. Anisotropy is a comparison between the amount of plane polarized light that excites the

complex and the amount which is emitted perpendicularly to the light used to excite the

molecule. In order to measure fluorescence anisotropy, emitted light is measured using a

polarizing filter oriented parallel to the polarized excitation light, $I_{//}$, and then measured

using polarized filters perpendicular to the exciting light, $I_{\perp}$. These measured emission

intensities are then used to calculate the molecule's anisotropy, r, using Equation 1,

which is a ratio of the polarized emission relative to the total emission:

$$r = \frac{I_{||} - I_{\perp}}{I_{||} + 2I_{\perp}} \tag{1}$$

Major factors in the anisotropy of a complex are its ability to undergo rotational

diffusion and its dipole moment. A molecule present in a more viscous solvent will have

a rotational diffusion rate that is slower than the rate of emission and will emit light

parallel to the light used to excite it. Additionally, the dipole moment of the molecule

can be influenced by the rigidity and size of the molecule itself. A complex which cannot

move easily will not be able to reorient itself, leading to the molecule emitting light in the

same direction as the light of excitation.[22] This is of great importance to the LMOF

sensor design as the transition metal complex will be locked in place due to the rigidity of

the LMOF structure; changing the free movement of the molecule, thus changing its

anisotropy.

Furthermore, the polarity of a molecule's environment can change the emission

properties of luminophores. When a molecule is in its excited state, its dipole moment

typically increases relative to the ground state. A polar solvent can increase the stability

of the polar molecule in that excited state, resulting in a lowering of the energy of the

excited state and emissions at longer wavelengths. The opposite is then also true; a less

polar solvent cannot stabilize the excited molecule as well, causing the molecule to exist at a higher energy excited state and emit at shorter wavelengths from the Frank-Condon, or locally excited, state. Typically, only molecules with inherent polarity will exhibit this kind of behavior. As the luminophore is more stable in polar solvents, this means one complex can have different emission wavelengths in different solvent environments.[23]

As observed in the literature, a mixture of solvents for a polar complex creates a distribution of excited state lifetimes of the complex present in the solution, resulting in an observed emission that is somewhere between the emission of the complex in each solvent alone.[23] This distinctively different behavior of polar compounds led to the proposition of using the complexes $[Os(CO)_2Cl_2(dcbpy)]$ and $[Os(CO)_2Cl_2(dcphen)]$, both of which have large dipole moments. Due to the solvent effects mentioned previously, it has been proposed that these complexes will exhibit this behavior when comparing their emissions in both polar and nonpolar solvents. The other two osmium complexes in this family do not have as large of a dipole moment but have larger α-diimine ligands, which red shift the emission wavelength and can vary the size of the pores in the LMOFs.

Particularly of importance in this research is how MOFs can be modified to create a luminescent metal-organic framework (LMOF). As previously stated, MOFs have a number of advantages over similar polymer and film-type support matrices. In regards to the preparation of LMOFs, they have distinct advantages over other methods, as they are easy to synthesize and form predictable structures, and their luminescence emissions are fully dependent on the choice of components used in the synthesis. The preparation of

16

LMOFs is relatively straightforward. A typical LMOF synthesis in dimethylformamide takes roughly a few hours to two days. Additionally, LMOFs prepared with similar components will likely have a similar crystal structure when formed. This allows for the prediction of the properties of LMOFs based on previously synthesized MOFs. While this particular work focuses on the integration of osmium transition metal complexes into LMOFs, literature has cited the integration of lanthanides and other transition metals. These LMOFs are not as useful for sensing as they emit in the near infrared region, which is harder to detect than UV-Visible radiation.[24]

As mentioned previously, it is the metal ions and organic linkers that combine to form the three-dimensional crystal structure in a MOF. A distinction between LMOFs prepared in the current work and traditional MOFs is that the carboxylated aromatic groups on the luminescent transition-metal complexes take the place of the organic linkers in the traditional approach.[9] Attempts are made to prepare two different types of LMOFs in the current work; and they are referred to as doped LMOFs and stoichiometric LMOFs. Doped LMOFs can be formed when substituting a small amount of the luminescent TMC for the organic linker in the synthesis. This allows for the extension of the network by both the organic linker present and the carboxylated aromatic rings on the TMCs.[25] In comparison, the stoichiometric LMOF is formed when there is a stoichiometric amount of the metal ion and the TMC. This should result in the replacement of every organic linker to be replaced by the carboxylated groups on the TMC.

Prototype LMOF Sensors for Measurement of O₂

To test the feasibility of the sensing model proposed in the current work, the capabilities of the transition metal complexes incorporated in luminescent metal-organic frameworks were investigated. In particular, because of its widespread usage, luminescence-based oxygen sensing using TMCs of the type proposed here is a useful way of assessing the validity of the proposed approach. Oxygen, which functions as a collisional quencher, quenches the luminescence of the metal complexes based on the Stern-Volmer equation, found in Equation 2 and 3:

$$\frac{I_0}{I} = \frac{\tau_0}{\tau} = 1 + K_{SV}[Q] \tag{2}$$

$$K_{SV} = k_q \tau_0 \tag{3}$$

In this equation, I_0 is the intensity in the absence of quencher, I is the intensity in the presence of quencher, k_q is the bimolecular quenching rate constant found in Equation 3, and Q is the concentration of the quencher. This same equation can be written as a function of the excited state lifetimes with and without quenching, τ and τ_0.[26]

While an ideal oxygen sensor exhibits a linear Stern-Volmer plot based on Equation 2, many oxygen sensors exhibit nonlinear Stern-Volmer plots which are rationalized by a "two-site" Stern-Volmer quenching model. This indicates that quenching is not uniform through the matrix when in the doped LMOF structure as the TMC is spread unevenly throughout the MOF structure.[26] It is anticipated that one type of MOF will exhibit the uniform emissions while the other will exhibit nonuniform emissions. The type of LMOF expected to quench non-uniformly throughout is what is

considered a doped LMOF, or one with small amounts of the luminescent transition metal complex compared to the metal linker ion.[27] The non-uniform quenching is expected as the transition metal is not evenly dispersed throughout the LMOF, thus causing a non-linear Stern-Volmer quenching plot.

Previous work related to luminescence-based sensors in polymer supports have indicated the trends of nonuniform emissions in related support matrices. Using fluorescence microscopy, it has been determined that specific sections of the polymer had greater emission intensity and were quenched more than other sections of the polymer. This resulted in a two-site fit to the Stern-Volmer quenching model, much like what is expected to be seen in the doped LMOF structure.[28] On the other hand, a stoichiometric version of the LMOF contains an equal ratio of the transition metal complex to the metal linker ion. It is anticipated this LMOF will exhibit more uniform quenching as the luminescent transition metal complex is equally spread throughout the LMOF.

The current work thus involves the synthesis of the osmium transition metal complexes $[Os(bpy)_2(dcbpy)]Cl_2$, $[Os(phen)_2(dcphen)]Cl_2$, and $[Os(CO)_2Cl_2(dcbpy)]$, as well as the photophysical characterization of these complexes. Further work regarding this project will also involve the synthesis of $[Os(CO)_2Cl_2(dcphen)]$ and complexes with additional systematic changes. The characterization includes the analysis of the luminescence properties of the solid of each complex and when the complex is dissolved in solvents of varying polarity, included in environments of different rigidity, and dissolved in solutions of varying pH. In future studies of the complexes, they will be incorporated into MOFs, and the photophysical properties of the LMOFs will be

determined. To test the ability of successful LMOFs to function as chemical sensors,

they will be used as an oxygen sensor to determine if the Stern-Volmer quenching plot

follows a linear or two-site quenching model.

EXPERIMENTAL

<u>Materials</u>

Ammonium hexachloroosmate (99.9%) was obtained from Alfa Aesar.

Formaldehyde (37% in 10-15% methanol), dichloromethane (99,8%), 4,4'-dicarboxy-

2,2'-bipyridine (98%), and dimethylformamide (99.8%) were obtained from Acros.

Formic acid (37%), 2-propanol (Certified ACS Plus), hydrochloric acid (conc.), sodium

hydroxide solution (50% wt./wt.), and $Zn(NO_3)_2 \cdot 6H_2O$ were purchased from Fisher

Scientific. 4,4'-Bipyridine was obtained from TCI, and 1,10-phenanthroline-4,7-

dicarboxylic acid was purchased from Arc Pharm, Inc. The metal complexes

$[Os(bpy)_2(dcbpy)]Cl_2$ and $[Os(phen)_2(dcphen)]Cl_2$ were obtained from a previous

synthesis by Ricky Castro. All reagents were used as received and collected as hazardous

waste, as appropriate.

<u>Methods</u>

Synthesis of $[Os(CO)_2Cl_2]^{2+}$, precursor to $[Os(CO)_2Cl_2(dcbpy)]$

To prepare the complex $[Os(CO)_2Cl_2]^{2+}$, the procedure proposed by van Slageren

and Stufkens was followed.[29] To a 100 mL Schlenk flask, 803.1 mg (0.95 mmol) of

ammonium hexachloroosmate was added. The flask was placed on the Schlenk line,

evacuated, and flooded with nitrogen for approximately 40 minutes. To the flask, 80 mL

(0.87 mmol) of formic acid and 30 mL (0.50 mmol) of formaldehyde were added to the

dark red $(NH_4)_2OsCl_6$ powder, resulting in a brownish red solution. As the sample

mixture was heated to 100°C, the solution became yellowish-brown. The solution was

heated for three days at 102.5°C and progressed to a yellow color without any evidence of solid.

The solvent was removed en vacuo on a rotary evaporator, leaving a white solid. The resulting solid was triturated with approximately 40 mL of dichloromethane and allowed to stir for approximately 1.5 hours. The solution turned yellow, leaving a white solid. The yellow solution was removed from the solid by vacuum filtration. To this resulting yellow liquid, approximately 40 mL of acetone was added and the solution placed on low heat to remove a majority of the solvent. The remaining solvent was evaporated off over the course of two days in order to form crystals. Yellow-brown crystals formed on the bottom of the Erlenmeyer flask. The product was analyzed by IR spectroscopy using the Nicolet iS10 FT-IR spectrometer with the ATR accessory.

The product was recrystallized by first dissolving the yellow crystals in 40 mL of dichloromethane to form a yellowish amber solution. To this solution, 40 mL of acetone was added, and it was placed on low heat to evaporate the solvent. After most of the solvent evaporated, the solution was allowed to sit overnight to fully remove the solvent. This recrystallized product was lighter in color than the original crystals. The sample was analyzed with IR spectroscopy using the Nicolet iS10 FT-IR spectrometer with the ATR accessory.

This procedure was repeated to make more of the $[Os(CO)_2Cl_2]^{2+}$ needed. After repeating the process, it was determined that the synthesis in which the reaction was allowed to progress for four days as compared to three days was the most successful of

the syntheses. In terms of yields, the reaction progressing for four days produced a 40%

yield while the reaction progressing for three only yielded 17.8% product.

Synthesis of [*Os(CO)₂Cl₂(dcbpy)*]

In order to prepare [Os(CO)$_2$Cl$_2$(dcbpy)], 89.9 mg (0.37 mmol) 4,4'-dicarboxy-

2,2'-bipyridine and 101.9 mg (0.32 mmol) of the previously synthesized [Os(CO)$_2$Cl$_2$]$^{2+}$

were added to a 100 mL round-bottom flask in 16 mL 2-propanol, similarly to a literature

procedure for a similar complex.[29] The solution was refluxed at 90 °C for 8 hours,

changing from a sandy brown color to a yellow liquid with a white solid remaining. This

reaction was monitored using infrared spectroscopy measurements at 4, 6, 7, and 8 hours.

A small portion of the solution was obtained, and the solvent was evaporated in order to

measure the solid via ATR-FTIR. The solvent was removed using heat after the peaks

corresponding to the starting materials disappeared and peaks corresponding to the

products appeared. Once all starting material peaks had disappeared and product peaks

were seen, a final infrared spectrum was recorded of the unpurified product.

In order to purify the product, it was dissolved in a small amount (10 mL) of

acetonitrile and a yellow solution separated from white powder. The yellow solution was

filtered off of the powder and the solvent was removed over heat to form yellow crystals.

An infrared spectrum was obtained using the ATR sample cell. This reaction yielded

4.5% and 10% for two different syntheses.

Synthesis of [Os(bpy)₂(dcbpy)]Cl₂

To prepare the final product, [Os(bpy)$_2$(dcbpy)]Cl$_2$, the precursor [Os(bpy)$_2$Cl$_2$]

needed to be synthesized. To a Schlenk flask, 20 mL of ethylene glycol was added and

purged with nitrogen gas. To this flask, 300 mg (0.683 mmol) of $(NH_4)_2OsCl_6$ and 214 mg (1.39 mmol) of 2,2'-bipyridine were added under nitrogen. A reflux was run at 200-210 °C for 45 minutes. The solution first became red with a yellow tint but became purple over the course of the reaction. It was then cooled to slightly above room temperature and 20 mL of sodium hydrosulfite solution was added. This solution was then placed in the freezer overnight.

To a 25 mL round bottom flask, 44 mg (0.180 mmol) of 2,2'-bipyridine-4,4'-dicarboxylic acid (dcbpy) was added, along with 6 mL of water. As the dcbpy did not dissolve readily in water, 0.25 mL of NaOH was added to the solution, and it turned brown. Small particles were formed, and 0.125 mL of HCl was added to the solution to dissolve the dcbpy. To this solution, 0.090 g (0.174 mmol) of $[Os(bpy)_2Cl_2]$ was added and the solution was stirred, turning reddish purple after 20 minutes. The solution was refluxed around 100°C for 2 hours and then removed using heat. The solvent was removed from heat and 6 mL of ethanol was added to the solid. The solution was placed in the freezer overnight and was filtered using a fine fritted glass filter. The yield for this reaction was about 85%.

Photophysical Characterization of Metal Complexes in Solution and Solid State

In order to characterize the luminescence properties of the complexes $[Os(bpy)_2(dcbpy)]Cl_2$, $[Os(phen)_2(dcphen)]Cl_2$, and $[Os(CO)_2Cl_2(dcbpy)]$, a small amount of the complex (~1 mg) was dissolved in various solvents, including water, acetonitrile, and a 50:50 mix of the two solvents. The maximum absorption wavelength for each complex in solution was determined using the Shimadzu UV-2401PC UV-Visible

spectrophotometer over the UV-Visible region from 200 to 700 nm. Excitation and emission spectra were obtained for the complexes in water, acetonitrile, and 50:50 acetonitrile:water using a Horiba Jobin Yvon Fluorolog-3 spectrofluorimeter.

Excitation and emission spectra for the metal complexes are obtained using a specific process utilizing the maximum absorbance wavelength. The complex is first excited at the maximum absorbance wavelength to obtain the emission spectrum. From the emission spectrum, the maximum emission wavelength is determined and then used to obtain an excitation spectrum for the complex. This allows for the optimum excitation wavelength to be determined. Once this wavelength is found, the emission spectrum of the complex is once again obtained using this maximum excitation wavelength.

Additionally, to determine the effects of pH on the emission of the complexes $[Os(bpy)_2(dcbpy)]Cl_2$ and $[Os(CO)_2Cl_2(dcbpy)]$, emission spectra were recorded under varying pH conditions in aqueous solution in order to determine the protonation state of the dicarboxylated ligand in solution. For the acidic measurements, two 2 μL aliquots of 6M HCl were added to sample in water and mixed. The solution was neutralized using 4 μL 6M NaOH, and the emission spectrum was obtained for this pH. To achieve basic conditions, two 2 μL of 6M NaOH were added to the neutral sample solution. Slit widths were determined by starting with 5 nm and adjusting upwards to obtain a signal in the range of 500,000-1,000,000 CPS. As the cause behind the maximum emission wavelength was unknown, the acid-base testing utilizing $[Os(bpy)_2(dcbpy)]Cl_2$ was continued by adding acid to the sample and the intensity of the combination peak was monitored to see if it decreased.

The emission and excitation spectra were obtained for each solid complex to compare it to the complex in pure solvents and solution. In order to perform this experiment, a small amount of the complex (~2 mg) was sandwiched between two quartz slides in the Horiba solid state sample holder. The emission and excitation spectra were obtained in front-face rather than right angle mode for the emission detector.

Preparation of Luminescent Metal Organic Frameworks

In order to prepare doped metal-organic frameworks, 0.033 g (0.1 mmol) $Zn(NO_3)_2 \cdot 6H_2O$, 0.008 g (0.05 mmol) 4,4'-bipyridine, 0.023 g (0.095 mmol) 1,10-phenanthroline-4,7-dicarboxylic acid, and 0.005 mol of metal complex were mixed in a 30 mL sample vial with 10 mL dimethylformamide (DMF). After ensuring that the compounds were thoroughly mixed in the vial, the vial was placed in an oil bath at 90°C for three to four days in order to form the MOF. The crystals that formed were filtered out of the DMF, and the vial was washed with excess DMF in order to ensure that the crystals were fully removed from the vial. The crystals were placed in a 25 mL round bottom flask and heated at 60-70 °C under vacuum for 24 hours to activate the crystals.

RESULTS AND DISCUSSION

Preparation of [$Os(CO)_2Cl_2(dcbpy)$]

[Os(CO)₂Cl₂]²⁺ Precursor. The complex [$Os(CO)_2Cl_2$]²⁺ was synthesized as it is the first step in the synthesis of the desired complex [$Os(CO)_2Cl_2(dcbpy)$]. Appendix 2 shows the infrared spectrum of the unpurified crystals from the first synthesis of precursor, [$Os(CO)_2Cl_2$]²⁺. The peaks indicating the formation of the intended product, [$Os(CO)_2Cl_2$]²⁺, lie at 2118 cm⁻¹ and 2004 cm⁻¹, which are similar to the literature values of 2117 cm⁻¹ and 2022 cm⁻¹.[21] These peaks correspond to the carbonyl groups on the osmium metal center and the minor shifts in wavenumbers could be due to impurities found within the sample. After the trituration process of the first synthesis was repeated, the infrared spectrum in Appendix 3 was obtained. The major peaks are observed at 2118 cm⁻¹ and 2020 cm⁻¹ in close agreement with the literature.[29] The typical yield of this reaction, completed four times, ranges from 18 to 40%, which is lower than the literature yields. Syntheses with a longer time for the reaction to occur yielded the most product. Additionally, having the complex and reagents under nitrogen for a longer period of time could help increase the yield of the complex.

Synthesis of [Os(CO)₂Cl₂(dcbpy)]. This particular complex was synthesized in order to prepare a complex with a large dipole moment, compared to the previously synthesized [$Os(bpy)_2(dcbpy)$]²⁺ and [$Os(phen)_2(dcphen)$]²⁺. Before beginning the synthesis of [$Os(CO)_2Cl_2(dcbpy)$], the infrared spectra were obtained for the two starting materials, 4,4'-dicarboxy-2,2'-bipyridine and [$Os(CO)_2Cl_2$]²⁺. As the reaction progressed for eight hours, it was followed using infrared spectroscopy. When the starting material

27

peaks began to disappear and product peaks formed, the reaction was removed from the heat, as seen in Appendix 3 and 4 for $[Os(CO)_2Cl_2]^{2+}$ and $[Os(CO)_2Cl_2(dcbpy)]$, respectively. After removing the solvent from the sample, the infrared spectrum in Appendix 4 was obtained. In the article by Janis et al, infrared stretches at 2046, 1975, and 1743 cm^{-1}, corresponding to the carbonyl groups, were reported as indicative peaks of the formation of the $[Os(CO)_2Cl_2(dcbpy)]$ product.[18] From Appendix 5, peaks at 2032, 1932, and 1704 cm^{-1} seem to correlate with these literature values and indicate the presence of the $[Os(CO)_2Cl_2(dcbpy)]$ product. However, the differences between the two infrared spectra may be because the literature source reported a polymer structure of this complex where this reaction did not create this extended structure. The reaction resulted in yields ranging from 4.5% to 10%. Additional product could be yielded if the reaction were allowed to proceed for a longer period of time and if the recrystallization process was optimized.

Characterization of Complexes in Solution

Dcbpy ligand. The emission spectrum for the dcbpy ligand was obtained by scanning from 340 to 600 nm with slit widths of 5 nm at an excitation of 315 nm, as seen in Figure 5. The maximum emission wavelength was determined to be 408 nm. The excitation spectrum was obtained by setting an emission wavelength of 408 nm and scanning from 200 to 395 nm with slit widths of 5 nm. The maximum excitation wavelength was determined to be 328 nm. The peak appearing around 360 nm in both the excitation and emission spectra is a Raman scatter peak present for water.
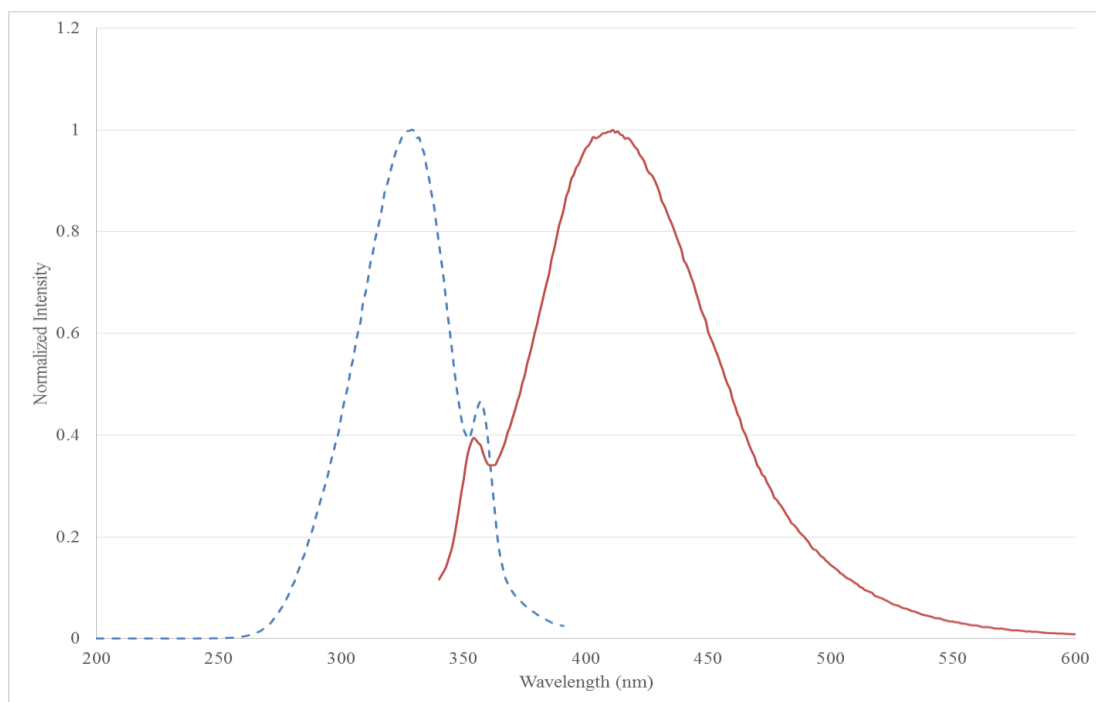
Figure 5. Excitation (- -) and emission(—) spectra for the dcbpy ligand in aqueous solution

Dcphen ligand. The emission spectrum for the dcphen ligand was obtained by scanning from 340 to 610 nm with slit widths of 5 nm at an excitation of 315 nm. The maximum emission wavelength was determined to be 398 nm. The excitation spectrum was obtained by setting an emission wavelength of 398 nm and scanning from 200 to 385 nm with slit widths of 5 nm. The maximum excitation wavelength was determined to be centered around 325 nm. The three different peaks appearing in Figure 6 occur due to the different vibronic transitions, caused by changes in both vibrational and rotational structure, of a single electronic state. Furthermore, this follows the trend predicted as the extended pi system of the dcphen ligand results in a lower energy needed to excite the complex and therefore a longer excitation wavelength.
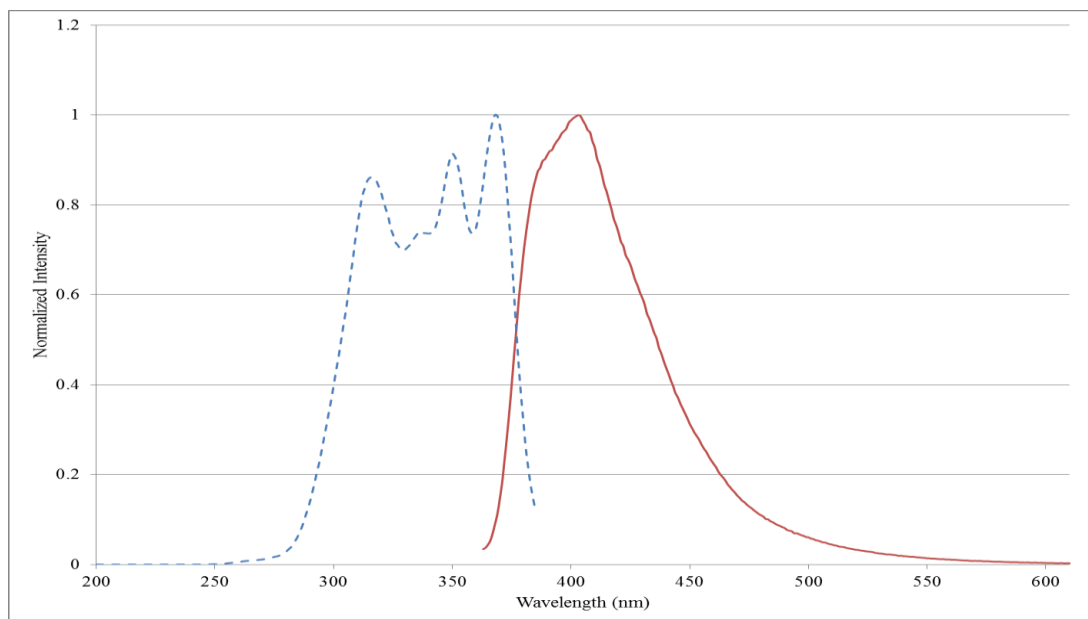
Figure 6. Excitation (- -) and emission(—) spectra for the dcphen ligand in aqueous solution

[Os(bpy)₂(dcbpy)]Cl₂. In order to characterize the different transition metal complexes, the absorbance spectrum was obtained for each complex, scanning from 200 to 700 nm, as seen in Figure 7. This absorbance wavelength maximum was used as an initial excitation wavelength parameter. For the [Os(bpy)₂(dcbpy)]Cl₂ complex, there were three different maximum absorbance wavelengths; 243 nm, 289 nm, and 403 nm. The lower wavelength absorbances are likely ligand-localized $\pi \rightarrow \pi^*$ transitions resulting from the two different α-diimine ligands on the complex, and the peak with a maximum absorption wavelength at 403 nm can be attributed to the metal to ligand charge transfer for the complex. In the inset of Figure 7, the MLCT absorption band can be seen easily as it spans from 350 to 550 nm.
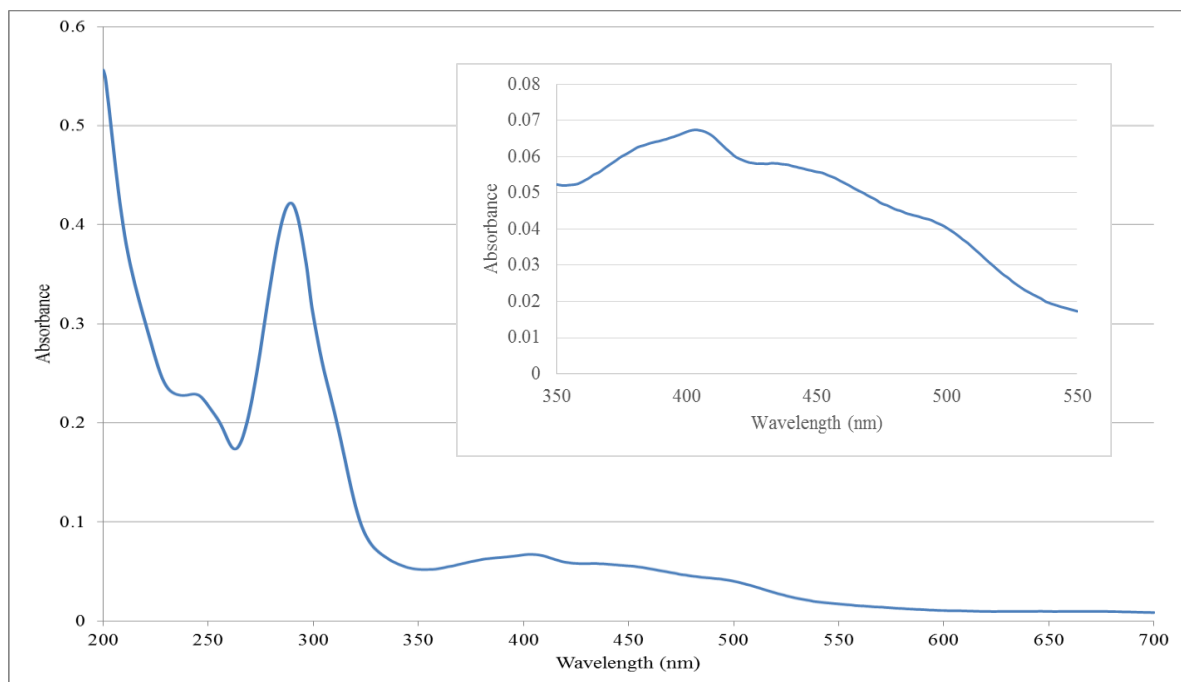
Figure 7. Absorbance spectrum for [Os(bpy)$_2$(dcbpy)]Cl$_2$ complex

To obtain the emission spectrum of [Os(bpy)$_2$(dcbpy)]Cl$_2$, the excitation wavelength was set to 450 nm with 8 nm slit widths on the excitation monochromator and scanned from 475 to 850 nm with 8 nm slit widths on the emission monochromator, as seen in the normalized spectrum in Figure 8. This produced two distinct peaks with maximum emission wavelengths of 627 nm and 740 nm. The peak at 740 nm exhibited greater emission intensity. These two peaks likely correspond to two different excited states the molecule can occupy, and the peak around 740 nm is the peak corresponding to the excited state that is more significantly populated. In this spectrum, the peak around 627 nm can be attributed to an excited state that is localized on the dcbpy ligand of the complex while the peak at 740 nm can be attributed to an excited state that is localized on the bpy ligand. This is notably seen in the literature as the maximum emission

31

wavelength for $[Os(bpy)_3]^{2+}$ is 743 nm, similar to the longer wavelength emission from the $[Os(bpy)_2(dcbpy)]^{2+}$ complex. This suggests that the dcbpy ligand, with a lower emission wavelength, is the higher energy excited state. This results from the carboxylated ligands pulling electron density away from the metal center, which would increase the amount of energy required to cause the MLCT to occur.

The excitation spectrum, found in Figure 8, was obtained by setting the emission wavelength to 627 nm with 8 nm slit widths on the emission monochromator and scanning from 330 to 600 nm and 8 nm slit widths on the excitation monochromator. This resulted in a maximum excitation wavelength of 417 nm. An excitation spectrum was also obtained for the second emission peak by setting the emission wavelength to 741 nm with 8 nm slit widths on the emission monochromator and scanning from 395 to 725 nm and 8 nm slit widths on the excitation monochromator. From this spectrum, the maximum excitation wavelength was determined to be 417 nm. A peak around 467 nm appeared in both excitation spectra, which is an artifact of the source used in the fluorimeter.
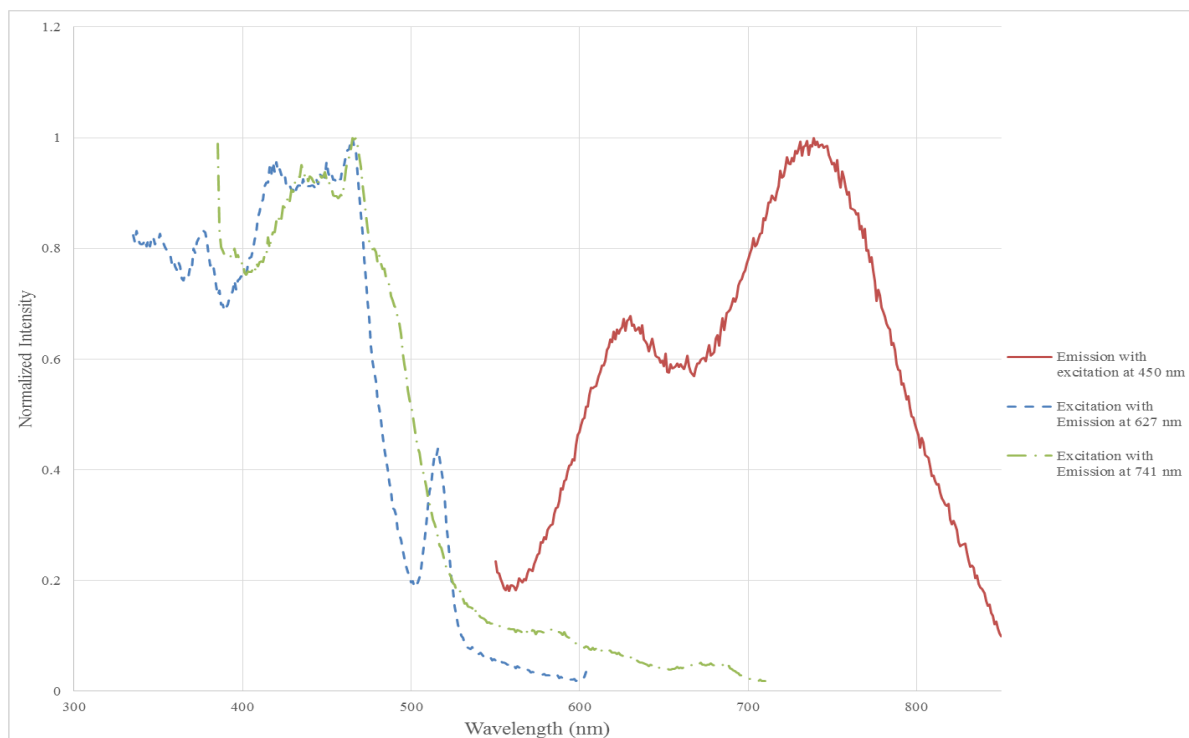
Figure 8. Excitation and emission spectra for [Os(bpy)$_2$(dcbpy)]Cl$_2$ complex in aqueous solution.

[Os(phen)$_2$(dcphen)]Cl$_2$. As seen in Figure 9, the absorbance spectrum of

[Os(phen)$_2$(dcphen)]Cl$_2$ was obtained by scanning wavelengths from 200 to 700 nm with

5 nm slit widths. From this spectrum, the maximum absorbance wavelengths were

determined to be 266 nm and a large stretch from around 350 to 550 nm, the longer of

which is a result of the MLCT absorption, as seen in the inset of Figure 9. The

absorbance at shorter wavelengths results from the π→π* absorbance in the

phenanthroline ligand on the complex.

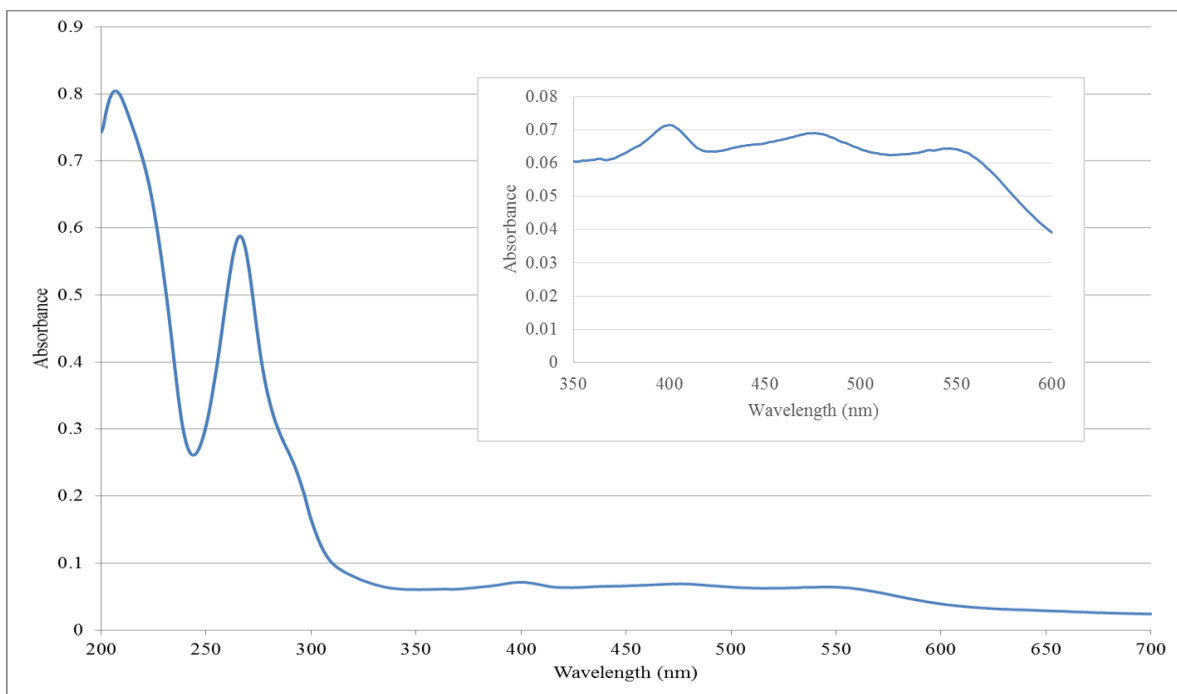**Figure 9.** Absorbance spectrum for for [Os(phen)$_2$(dcphen)]Cl$_2$ complex

In order to obtain the emission spectrum for the complex [Os(phen)$_2$(dcphen)]Cl$_2$, the complex was excited at 450 nm with 5 nm slit widths, which is expected to be the best excitation for the MLCT transition to occur. This resulted in emission peaks with maxima at 600 and 692 nm, likely due to emissions both from ligand-localized emission and the MLCT transition, respectively. The portion of the spectrum missing was a Raman scatter peak for water excited at 450 nm. In order to obtain the optimum excitation wavelength for the lower energy emission, the emission wavelength was set at 692 nm with 5 nm slit widths, as seen in Figure 10. The maximum excitation wavelength was determined to be 425 nm. The emission wavelength varies slightly lower than that of the complex [Os(bpy)$_2$(dcbpy)]Cl$_2$ as the phenanthroline ligands are slightly better electron withdrawing groups than the bipyridine ligand, which pulls electron density

34

away from the metal center. This causes an increase in energy for transitions to occur,

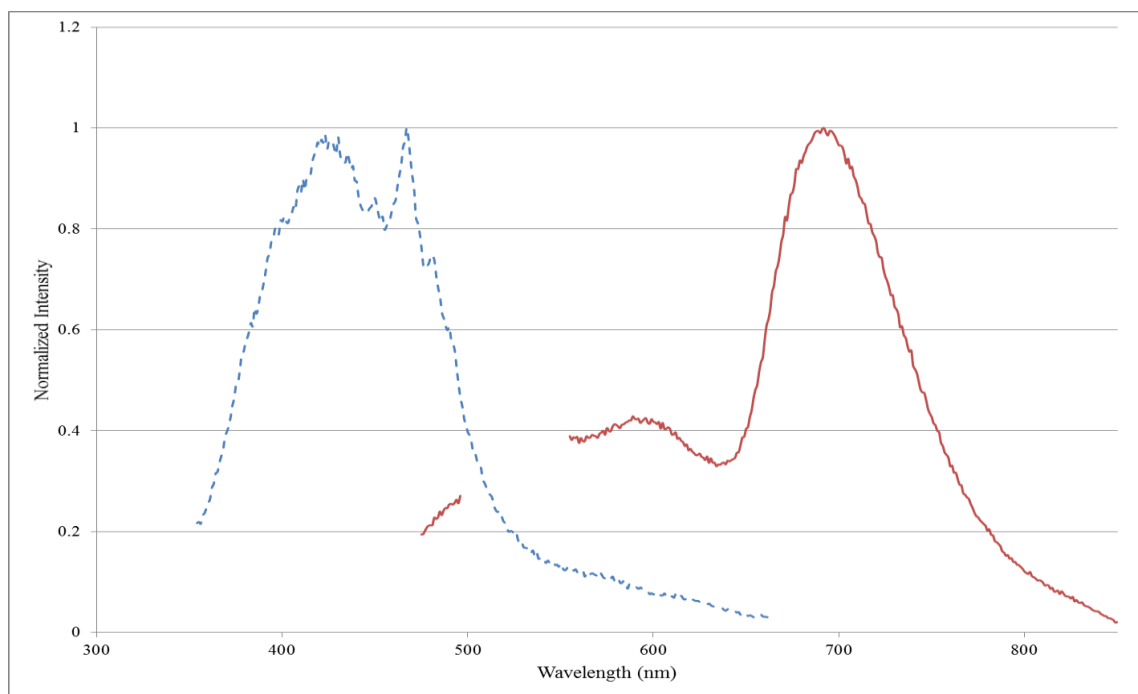resulting in shorter wavelengths, as seen in the dcbpy and dcphen compounds themselves.

Figure 10. Excitation (- -) and emission(—) spectra for [Os(phen)$_2$(dcphen)]Cl$_2$ complex in aqueous solution.

[Os(CO)$_2$Cl$_2$(dcbpy)]. The maximum absorbance of the MLCT for the complex

[Os(CO)$_2$Cl$_2$(dcbpy)] was initially found by finding the absorbance from 200 to 700 nm

with 5 nm slit widths, as seen in Figure 11. The maximum absorbance wavelength was

determined to be 315 nm with the absorbance stretching out past 400 nm, as seen in the

inset of Figure 11. This wavelength is consistent with the maximum absorption

wavelength of this complex (398 nm) reported in the literature.[18] The peak around 315 to

330 nm is the result of the π→π* transitions occurring within the ligand on the complex,

35

which is also consistent with the maximum ligand-localized emission at 315 nm found in the literature.[18]
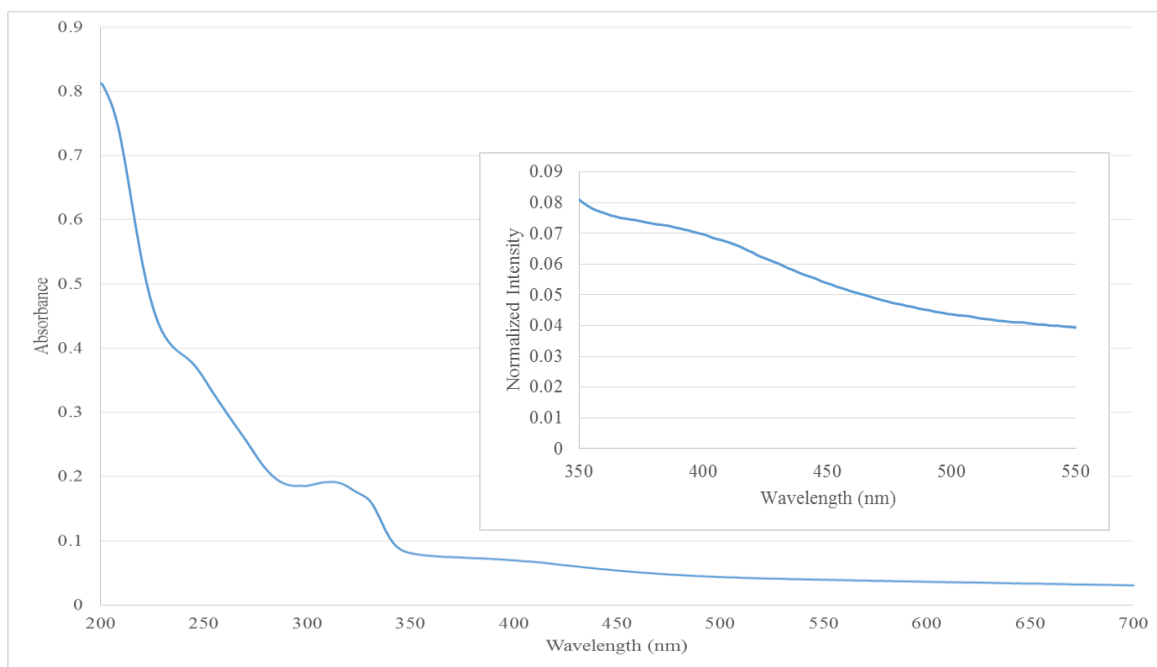

Figure 11. Absorbance spectrum of $[Os(CO)_2Cl_2(dcbpy)]$ complex

In order to obtain an emission spectrum for the complex, the complex was first excited at 398 nm, which is the literature and experimental absorbance maximum wavelength. This produced a maximum emission wavelength of 557 nm. Setting the emission monochromator at 557 nm with 8 nm slit widths and scanning from 290 to 545 nm with 8 nm slit widths on the excitation monochromator indicated the maximum excitation wavelength was 375 nm. The complex was then excited at 375 nm with 8 nm slit widths and the emission monochromator was scanned from 395 to 725 nm with 8 nm slit widths. Both can be seen in Figure 12.

From this emission spectrum, found in Figure 12, two maximum emission wavelengths were determined to be at 458 nm and 558 nm, both corresponding to

different MLCTs in the complex. It is likely that the emission at 458 nm is a result of the transition between the carbonyl groups and the metal center as the transition with a carbonyl group is of higher energy, and thus shorter wavelengths, than a transition between the metal center and dcbpy. This result is consistent with previous work done by the research group when investigating similar complexes and with the spectrum obtained for $[Os(bpy)_2(dcbpy)]Cl_2$. In the emission spectrum for $[Os(bpy)_2(dcbpy)]Cl_2$, the dcbpy ligand emitted around similar emission wavelengths, 627 nm for that complex compared with 550 nm for this particular complex. As the complex contains two carbonyl groups, which increase the energy of all of the transitions in a complex, the excitation and emission wavelengths shift to lower wavelengths as a higher energy results in a shorter excitation or emission wavelength. The portion omitted from the emission spectrum was the result of a Raman scatter peak of water excited at 375 nm.
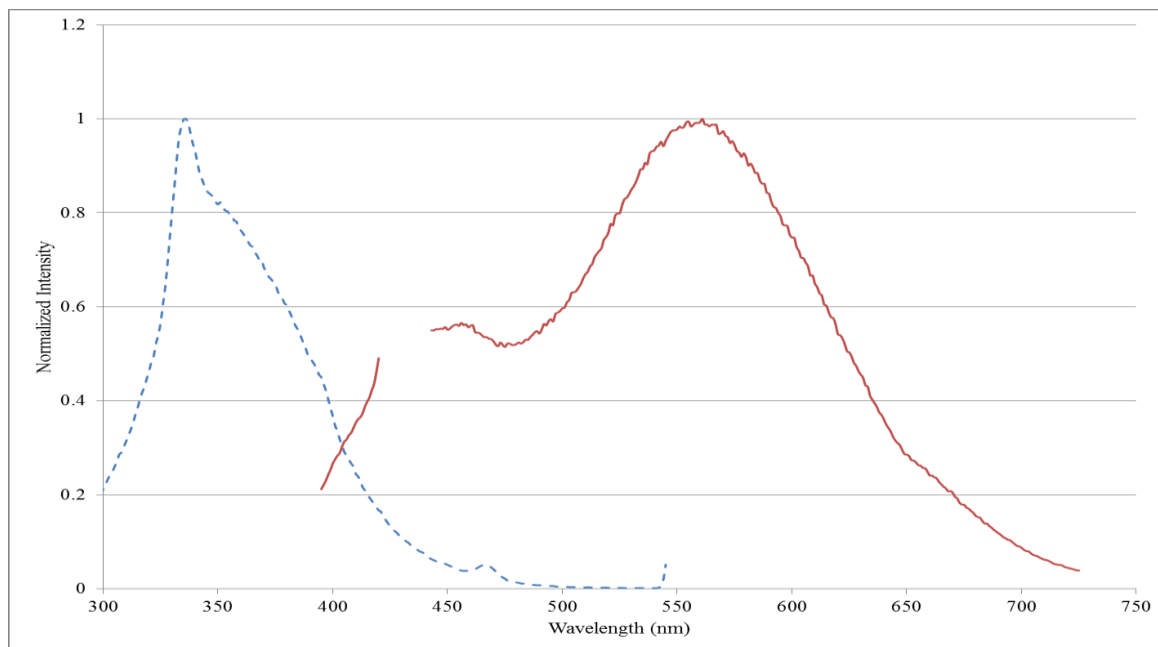

Figure 12. Excitation (- -) and emission(—) spectra for $[Os(CO)_2Cl_2(dcbpy)]$ complex in aqueous solution.

Solid-State Characterization of Complexes

Solid-state characterization was performed on the complexes in order to see the emissions of the complexes without any influence from solvents. The emission spectrum of $[Os(bpy)_2(dcbpy)]Cl_2$ in solid state was obtained by scanning from 475 to 850 nm with 8 nm slit widths, exciting at 450 nm, as seen in Figure 13. The maximum emission wavelengths for the two observed transitions were determined to be 525 and 685 nm, and the maximum excitation wavelength was determined to be 427 nm. As seen in solution, there are two peaks corresponding to the complex in solution, but they are shifted to shorter wavelengths for the solid as compared to the complex in solution. This occurs as the solvents stabilize the excited states of the complexes to a lower energy state, causing emissions at longer wavelengths. Comparatively, while the complex in solid state exhibits both peaks, the higher energy peak at 525 nm has a higher intensity.
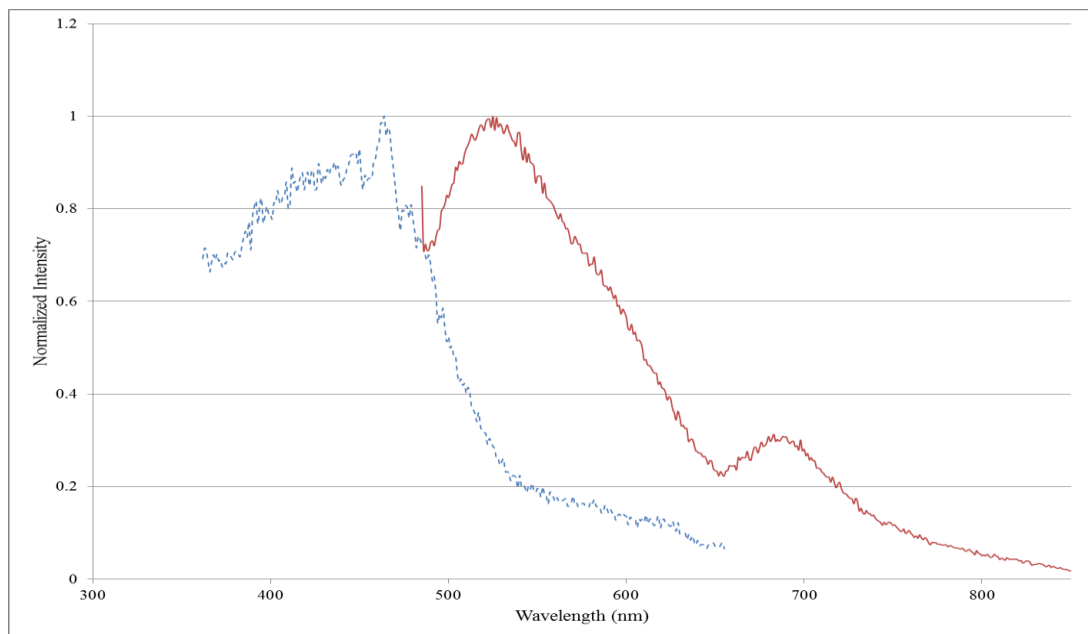

Figure 13. Excitation (- -) and emission(—) spectra for $[Os(bpy)_2(dcbpy)]Cl_2$ complex in solid state.

Similar spectral acquisition was repeated for the complex [Os(CO)$_2$Cl$_2$(dcbpy)] by measuring the emission and excitation spectra. The maximum emission wavelength was determined by exciting at 394 nm with slit widths of 5 nm and scanning from 410 to 750 with slit widths of 5 nm. The maximum emission wavelengths for the two emission peaks were determined to be 580 and 696 nm and the maximum excitation wavelengths were determined to be 394 and 448 nm, as seen in Figure 14. The two observed emission peaks can be attributed to the carbonyls and the dcbpy group on the complex, respectively. As the carbonyls are strong field ligands and withdraw electrons from the metal itself as they are good pi-acceptors, the inclusion of these ligands increases the splitting between the d to d* transitions. This causes a larger energy gap between the lower d energy of the metal center and the MLCT transition requires an increased energy to occur, causing the emission wavelength to be shifted to shorter wavelengths but making the complex more photostable. Additionally, each of the emission wavelengths has a unique excitation wavelength, which leads to the population of one excited state over another when exciting at each respective excitation wavelength.
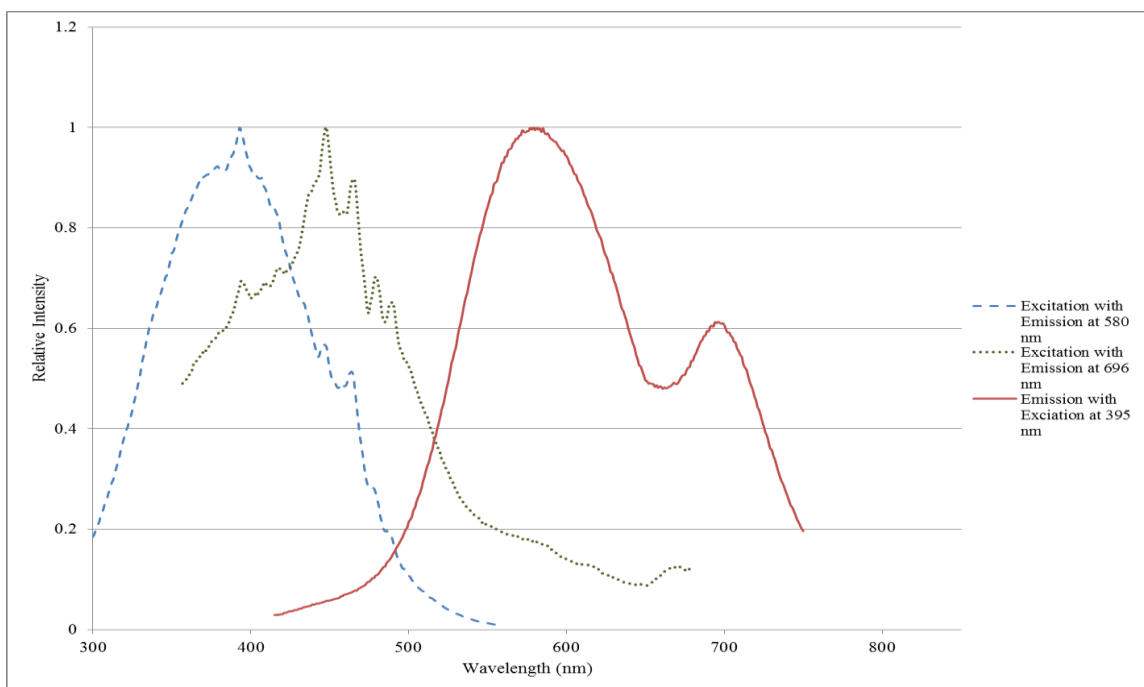
Figure 14. Excitation and emission spectra of [Os(CO)$_2$Cl$_2$(dcbpy)] in Solid State

Acid-Base Characterization of Complexes in Solution

[Os(bpy)$_2$(dcbpy)]Cl$_2$. To determine the effect of protonated carboxyl groups on the α-diimine ligands to total emission, a pH study was performed to change the amount of hydrogen and hydroxide ions present in solution with the complex. When performing acid-base studies on the [Os(bpy)$_2$(dcbpy)]Cl$_2$ complex, acid and base were systematically added to a neutral solution and the emission spectra were obtained, as seen in Figure 15. The complex was excited at 450 nm with 8 nm slit widths and the emission wavelengths scanned ranged from 475 to 850 nm with 8 nm slit widths. The region prior to 550 nm was removed due to the presence of a Raman scatter peak for water at 525 nm. Results reported have not been corrected for dilution of the solutions; slight decreases are

40

attributed solely to lower concentration of the complex upon the addition of acid or base.
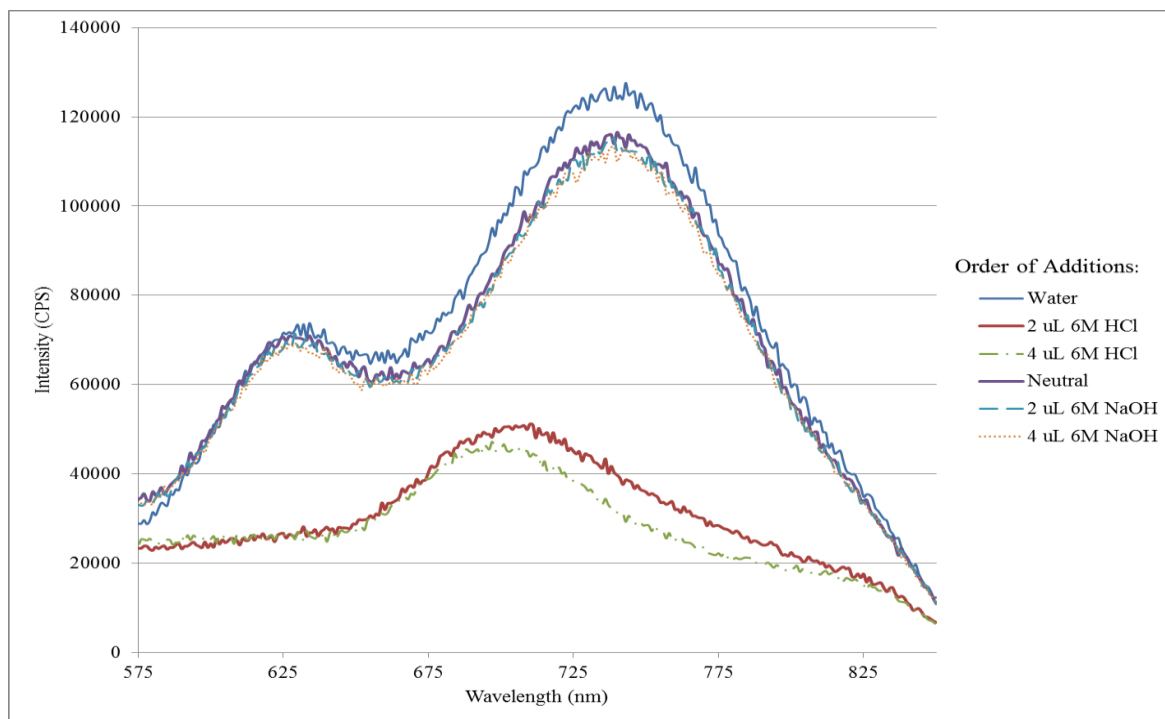

Figure 15. Emission spectra for acid-base additions for $[Os(bpy)_2(dcbpy)]Cl_2$ in aqueous solution, not corrected for dilution effects

In aqueous solution, $[Os(bpy)_2(dcbpy)]Cl_2$ exhibits two different emission peaks, attributed to dcbpy and bpy, respectively, as seen in Figure 15. There are two distinct peaks in this emission spectrum resulting from two different excited states. The acid base study raised the question as to what was occurring when acid was added to the complex in aqueous solution. Two potential explanations were discussed. In the first, it was suggested that the acid was causing one of the aromatic groups to dissociate from the metal in the complex. In the second, it was hypothesized the acid was protonating the carboxyl groups on the ligands, causing the two different ligands to have similar emission properties and form a peak with qualities of both ligands. To answer this question,

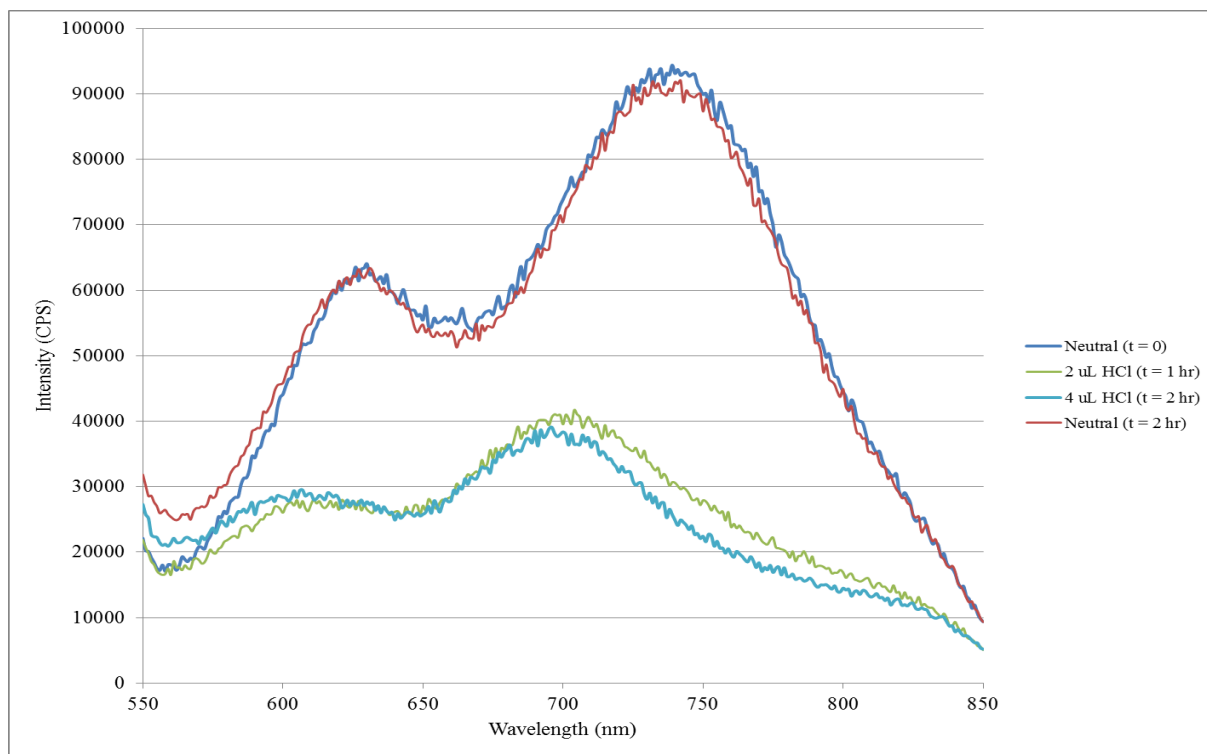another pH experiment was performed, as seen in Figure 16.

Figure 16. Additional pH study on [Os(bpy)$_2$(dcbpy)]Cl$_2$ in aqueous solution over time

If the first theory regarding the one peak present in acidic conditions was correct, this would indicate the intensity of the emission peak would decrease over the course of time as the complex would be dissociating. Based on the acid-base study shown in Figure 16, it was determined that the second of the two options is occurring as the intensity of the emission did not decrease over time. Furthermore, the [Os(bpy)$_2$(dcbpy)]Cl$_2$ complex must have predominately deprotonated carboxylic acid groups in its stable form in aqueous solution as the complex responded to the addition of acid with a change in emission wavelength. As more base was added to the solution, there was minimal change in the maximum emission wavelength, which indicates that the complex in a neutral solution is already deprotonated. It is anticipated that the

photophysical behavior observed in acidic solution is what will be observed for the complex when in the MOF, since the carboxylated ligand will be coordinated in the MOF just as the ligand is protonated in acidic conditions. When dissolved in water, the solution was yellow, and as more acid was added, the solution became darker in color. Through this study it was also determined that the maximum emission wavelengths for $[Os(bpy)_2(dcbpy)]Cl_2$ are 741 nm and 697 nm when in basic and acidic conditions, respectively, and the maximum excitation wavelength is 417 nm.

In the study of $[Os(phen)_2(dcphen)]Cl_2$ under similar acid-base additions, there was no change in the maximum emission wavelength from its expected emission wavelength of 690 nm and a slight second emission peak at 600 nm. The dcphen ligand has a lower pKa value than the dcbpy ligand, 0.62 versus 1.67, suggesting the hydroxyl groups on the dcphen ligand are protonated in water and adding acid to the complex would not cause a change in emission wavelength. This likely means that the dcphen ligand is acting like the phenanthroline ligand in solution.

$[Os(CO)_2Cl_2(dcbpy)]$. Similar spectral acquisition was performed on the $[Os(CO)_2Cl_2(dcbpy)]$ in acidic and basic conditions. Each emission spectrum was obtained by exciting at 375 nm with 8 nm slit widths on the excitation monochromator while scanning from 395 to 715 nm with 8 nm slit widths on the emission monochromator. An emission spectrum was obtained prior to any additions and after every addition of either 6M HCl or 6M NaOH, as seen in Figure 17.
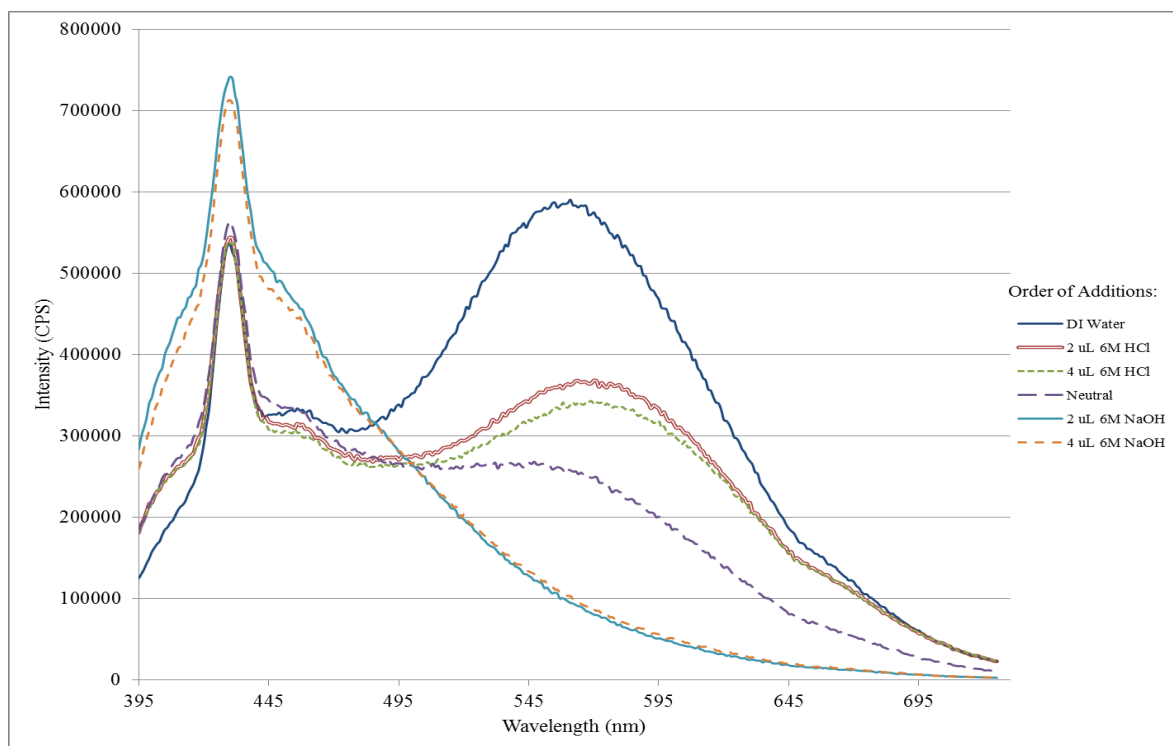
Figure 17. Emission spectra for acid-base additions for [Os(CO)$_2$Cl$_2$(dcbpy)] in aqueous solution, not corrected for dilution effects

In aqueous solution, [Os(CO)$_2$Cl$_2$(dcbpy)] has two different excited states present in its emissions spectrum, which are attributed to the carbonyl groups and dcbpy, respectively. As more acid was added, there was a shift in intensity of the two different excited states, with the peak around 550 nm completely disappearing upon addition of base. The peak appearing at 430 nm is a Raman scatter peak for water when excited at 375 nm. While it was determined the addition of acid to the [Os(bpy)$_2$(dcbpy)]Cl$_2$ complex in aqueous solution did not cause the dissociation of the complex, it seems that for [Os(CO)$_2$Cl$_2$(dcbpy)] this could be the case. Once the complex was added to basic conditions, the peak around 400 nm grew, indicating there could be free dcbpy ligand present as that is the emission wavelength of the dcbpy ligand, as seen in Figure 5. Comparing it to the previous study, the neutral solution containing the

[Os(bpy)$_2$(dcbpy)]Cl$_2$ complex had peak intensity similar to that of the complex in just water. However, in this particular experiment, the dcbpy peak in the neutral solution has an intensity of almost half of the plain DI water, which leads to the conclusion that this complex is not as stable as the [Os(CO)$_2$Cl$_2$(dcbpy)] in solutions of varying pH.

These acid-base experiments give insight into how the emissions of the complexes may change once in the LMOF structure. When incorporated into this structure, the transition metal complex is coordinated to a metal ion through the carboxyl groups on the α-diimine ligands. It is believed the complexes will have similar photophysical properties to when they are in their protonated form. From these experiments, it could be hypothesized that [Os(bpy)$_2$(dcbpy)]Cl$_2$ will have emissions at shorter wavelengths than seen when in aqueous solution. However, as [Os(phen)$_2$(dcphen)]Cl$_2$ did not change upon the addition of acid, which would ensure the carboxyl groups are protonated, this indicates the LMOF should have emissions similar to the complex in DI water.

Solvent Characterization of Complexes

[Os(bpy)$_2$(dcbpy)]Cl$_2$. The emission spectra of the complexes in solvents of different polarities were obtained in order to determine the environment sensitivity of the complexes. First, the complex was dissolved in acetonitrile and the complex, [Os(bpy)$_2$(dcbpy)]Cl$_2$, was dissolved in water, and the emission spectrum was obtained by exciting at 450 nm and scanning from 465 to 850 nm with 8 nm slit widths and can be found in Figure 18. The maximum emission wavelength was determined to be 730 nm, and the maximum emission wavelength was determined to be 445 nm.
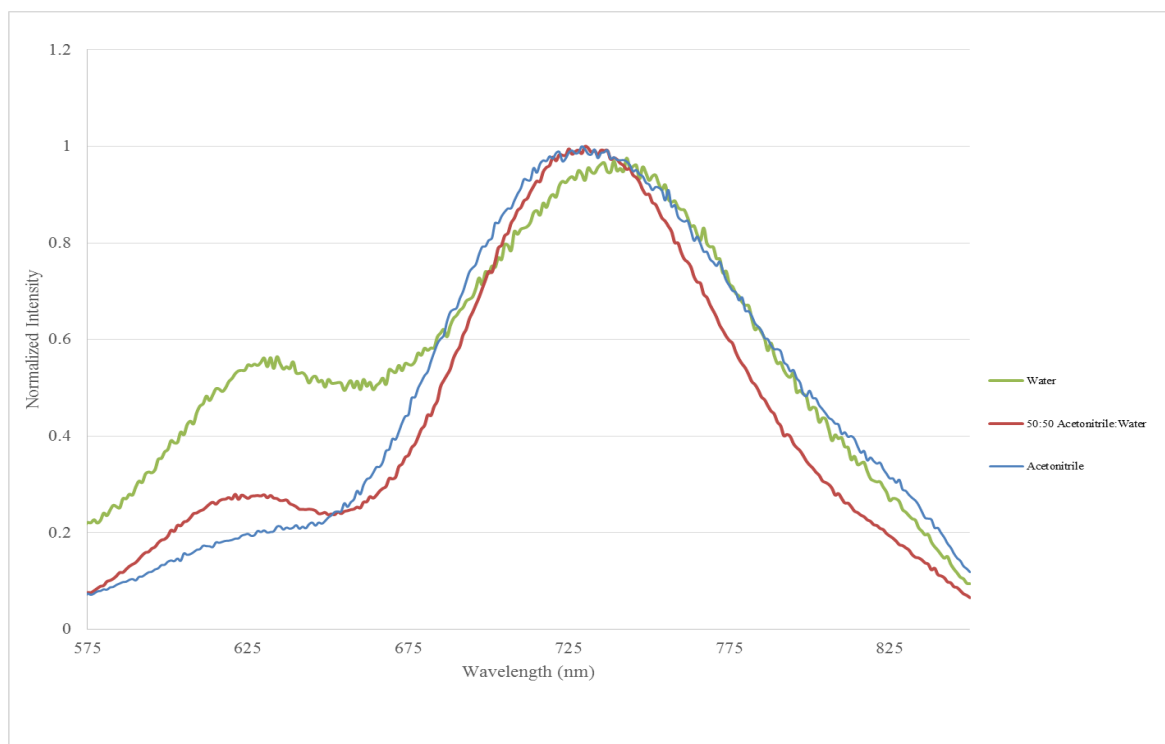
Figure 18. Emission spectra of $[Os(bpy)_2(dcbpy)]Cl_2$ in various solvents

This process was repeated using a 50:50 mixture of acetonitrile to water. The maximum emission wavelengths for this solvent system were determined to be 625 and 730 nm, and the maximum excitation wavelength was determined to be 441 nm. The maximum emission wavelength of the complex in water was previously determined to be 741 nm. In addition, the excitation spectrum was obtained by setting an emission wavelength at 741 nm and scanning from 360 to 650 nm with slit widths of 5 nm. Additionally, a peak appeared in water and 50:50 mixture which did not seem to be present in the acetonitrile spectrum. This peak was not dependent on the excitation wavelength and as indicated previously is an excited state originating from the MLCT between the osmium metal center and the dcbpy ligand. A ratio of these two peaks may give an indication of the polarity of the molecule, which requires further investigation.

[Os(phen)₂(dcphen)]Cl₂. This process was repeated with the complex $[Os(phen)_2(dcphen)]Cl_2$ by first dissolving the complex in acetonitrile and the same process was repeated. The maximum emission wavelength was determined to be 692 nm. The process was then repeated with the complex dissolved in a 50:50 acetonitrile: water mixture. The maximum emission wavelength was determined to be 692 nm for this solvent system, and the maximum emission wavelength was determined to be 425 nm for all three of the solvent mixtures. The maximum emission wavelength in water was determined to be 600 and 690 nm, which can be found in Figure 19. Similarly to the $[Os(bpy)_2(dcbpy)]Cl_2$, when the complex was dissolved in water, a peak around 600 nm appeared with relatively high intensity. As this peak did not change with different excitation wavelengths, it was determined this peak resulted from the MLCT between the osmium metal center and the dcphen ligand on the complex. However, the relative height of these peaks compared to one another is smaller than the two peaks of $[Os(bpy)_2(dcbpy)]Cl_2$, indicating the dcbpy excited state is more readily populated than the dcphen excited state as the complex itself is less sensitive to changes in its environment's polarity.
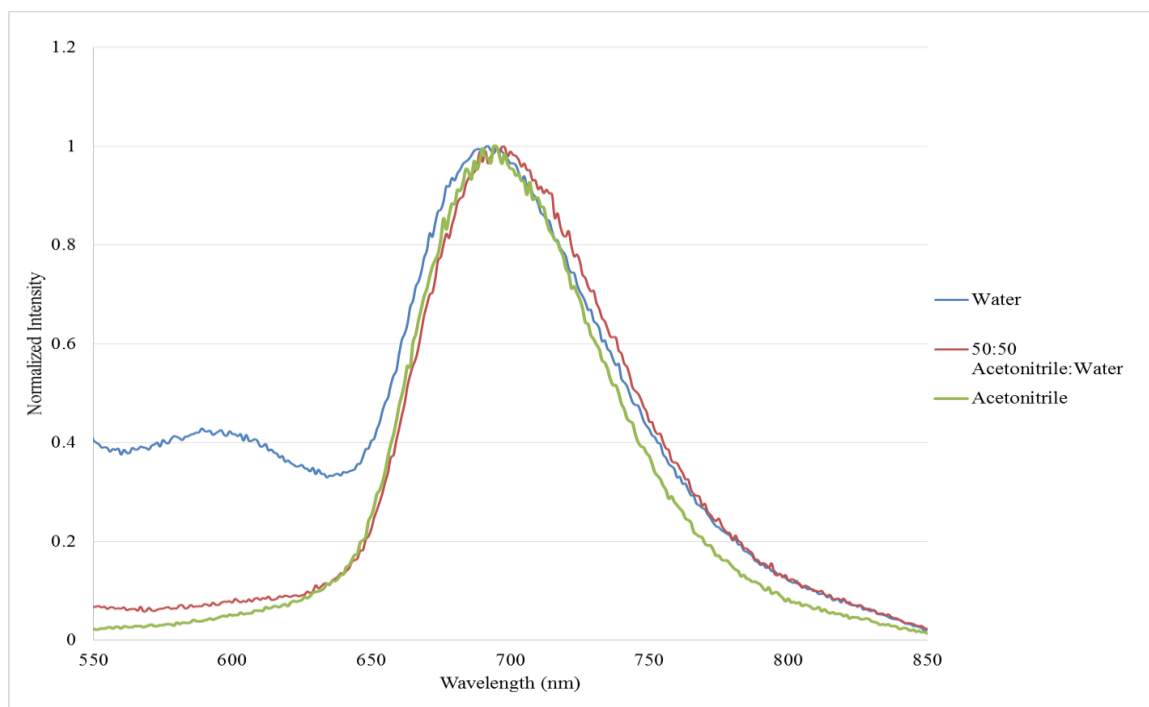
47

Figure 19. Emission spectra of [Os(phen)$_2$(dcphen)]Cl$_2$ in various solvents

[Os(CO)$_2$Cl$_2$(dcbpy)]. The complex [Os(CO)$_2$Cl$_2$(dcbpy)] was also subjected to

the same solvent testing as the other complexes with the same parameters used for the

complex in water by itself, as seen in Figure 20. In the differing solvents, the complex

was excited at 375 nm with 8 nm slit widths on the excitation monochromator and its

emission was scanned from 395 to 725 nm with 8 nm slit widths on the emission

monochromator. In water, the maximum emission wavelengths for the complex were

458 and 558 nm, resulting from interactions of the carbonyls and the dcbpy ligand and

the osmium metal center, respectively. In a 50:50 acetonitrile: water mixture, the

maximum emission wavelength was present at 517 nm. This indicates that the two

excited states are both equally populated and begin to have similar emission properties,

resulting in one combined emission peak. In acetonitrile, the complex was found to have

two maximum emission wavelengths, around 482 nm and 603 nm, attributed to the

carbonyls and the dcbpy ligand, respectively. The relative intensity of the signal also

indicates that both excited states are equally populated when in acetonitrile. The red shift

between the acetonitrile and water solvent systems is similar to that reported by the

literature for $[Os(bpy)_3]^{2+}$, in which the emission in water was 715 nm and the emission

in acetonitrile was 743 nm.[30] This is likely due to the electronic interactions between the

solvent and the complex itself, as the electrons can be localized in different parts of the

complex when in solvents of differing electronic composition.[31] Although the literature

reported a red shift of a similar complex to $[Os(bpy)_2(dcbpy)]Cl_2$ in acetonitrile, this

trend was not seen in the experimental results. However, the presence of the dcbpy

ligand produced a second peak which could have contributed to the shifting of the bpy
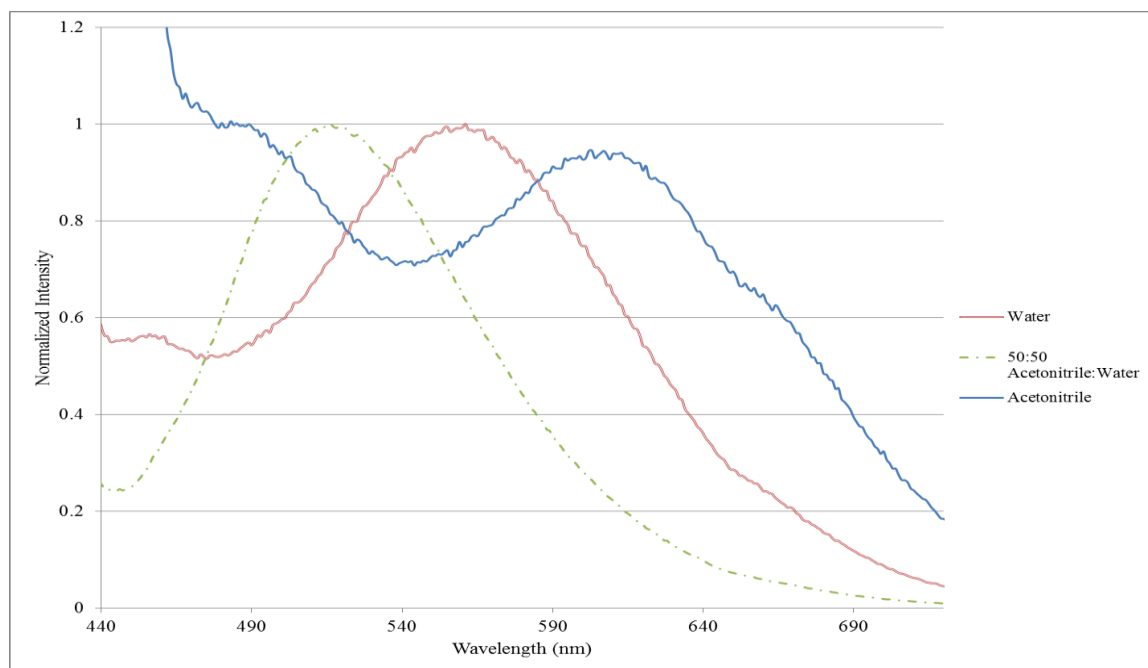
MLCT emission to longer wavelengths.

Figure 20. Emission spectra of $[Os(CO)_2Cl_2(dcbpy)]$ in varying solvents

Synthesis of Luminescent Metal-Organic Frameworks

In order to test our sensing method, the LMOF was first synthesized using a metal ion, $Zn(NO_3)_3$, and the transition metal complexes. Two different doped luminescent metal-organic frameworks were synthesized using the complexes $[Os(CO)_2Cl_2(dcbpy)]$ and $[Os(bpy)_2(dcbpy)]Cl_2$. Both syntheses resulted in product formation. However, the product of the synthesis utilizing $[Os(bpy)_2(dcbpy)]Cl_2$ was mostly powder with a few small crystals, but the crystals could not be separated easily from the powder, which may also be the LMOF itself. The LMOF resulting from the synthesis with $[Os(CO)_2Cl_2(dcbpy)]$ resulted in the formation of crystals but they were so small that they could not be obtained in order to be analyzed. In order to obtain better crystal formation, the reaction could be allowed to progress longer or special care could be taken in cooling the vials down to room temperature to ensure the crystals can precipitate out more effectively.

<u>Conclusions</u>

In this work, the photophysical properties of luminescent transition-metal complexes were analyzed in order to predict how they would emit once incorporated into a metal-organic framework. This involved studying the complexes in various solvent systems, in aqueous solution with varying pH, and in solid state. From these studies, it can be noted that these particular osmium metal complexes have two excited states, likely present due to the inclusion of two different ligands on the metal center. Based on the results obtained, it is likely that the higher energy excited state is prevalent when in polar solvents, in basic conditions, and when the complex is in solid state. This excited state corresponds to the MLCT localized on the dcbpy ligand and the emission at longer wavelengths is from the MLCT localized on the bipyridine ligand. More interestingly, this excited state seems more dominant when in solid state, which could be how the complexes emit when incorporated into an LMOF.

Prior research pertaining to this project has indicated that $[Os(phen)_2(dcphen)]Cl_2$ in an LMOF produces emissions similar to the complex itself in aqueous solution. However, this complex had a lower intensity of its higher energy excited state when in more polar solvents. This difference could indicate that $[Os(CO)_2Cl_2(dcbpy)]$ and $[Os(bpy)_2(dcbpy)]Cl_2$ will emit more at the lower energy excited state when integrated into an LMOF system as that excited state is more populated when in solid state and when in solutions of varying pH. Furthermore, when in acidic conditions, the emission of $[Os(bpy)_2(dcbpy)]Cl_2$ shifted to shorter wavelengths, which is likely how the complex will respond when in an LMOF system as it will be coordinating with the Zn metal ions

when integrated into the MOF, much like the effect of protonating the carboxylic acid groups on the dcbpy. Further experimentation needs to be performed on [Os(CO)$_2$Cl$_2$(dcbpy)] in order to fully determine its sensitivity to changes in its environment.

Initial results, however, point to the sensitive nature of the complexes to changes in their environment, which could lead to a sensitive and selective mechanism of optical sensing when integrated into the LMOF support matrix. Additionally, the characterization performed throughout this work can be utilized to predict the nature of the complexes upon integration into the LMOF.

Future Work

This family of complexes will be completed, with the synthesis of [Os(CO)$_2$Cl$_2$(dcphen)], to gain a fuller picture of the changes in photophysical properties which occur by varying the ligands on TMCs. Additionally, doped and stoichiometric LMOFs will be synthesized using all of the complexes in this family to see how these properties change once contained in MOF form. After the synthesis of these LMOFs, their response to oxygen will be measured and plotted using the Stern-Volmer equation. Once this analysis has been performed, changes to the LMOF system can be performed in order to begin sensing for analytes other than oxygen. This can be performed as the environment sensitivity of the complexes can change the selectivity of the LMOF for particular analytes. At this stage, it will likely be determined how much of the LMOF is actually necessary to perform such analyses and to see if the process of creating LMOFs can be scaled up for mass production. As stated previously, an advantage of optical

sensors is that only a small amount of the sensor is required to obtain an analysis. This would prove beneficial for sensing in the field as the required sensing mechanism is quite portable.

References

1.   Agati, G.; Tuccio, L.; Kusznierewicz, B.; Chmiel, T.; Bartoszek, A.; Kowalski, A.; Grzegorzewska, M.; Kosson, R.; Kaniszewski, S., Nondestructive Optical Sensing of Flavonols and Chlorophyll in White Head Cabbage (*Brassica oleracea* L. var. *capitata* subvar. *alba*) Grown under Different Nitrogen Regimens. *J. Agric. Food Chem.* **2016,** *64*, 85-94.

2.   Fong, J. K.; Pena, J. K.; Xue, Z.-L.; Alam, M. M.; Sampathkumaran, U.; Goswami, K., Optical Sensors for the Detection of Trace Chloroform. *Anal. Chem.* **2015,** *87*, 1569-1574.

3.   (a) Tellis, J. C.; Strulson, C. A.; Myers, M. M.; Kneas, K. A., Relative Humidity Sensors Based on an Environment-Sensitive Fluorophore in Hydrogel Films. *Anal. Chem.* **2011,** *83*, 928-932; (b) Qi, J.; Liu, D.; Liu, X.; Guan, S.; Shi, F.; Chang, H.; He, H.; Yang, G., Fluorescent pH Sensors for Broad-Range pH Measurement Based on a Single Fluorophore. *Anal. Chem.* **2015,** *87* (5897-5904), 5897; (c) McDonagh, C.; Burke, C.; MacCraith, B., Optical Chemical Sensors. *Chem. Rev.* **2008,** *108*, 400-422.

4.   Lakowicz, J. R., Fluorescence Sensing. In *Principles of Fluorescence Spectroscopy*, 3rd ed.; Springer: 2006.

5.   Higgins, B.; DeGraff, B. A.; Demas, J. N., Luminescent Transition Metal Complexes as Sensors: Structural Effects on pH Response. *Inorg. Chem.* **2005,** *44*, 6662-6669.

6.   Kneas, K. A.; Demas, J. N.; DeGraff, B. A.; Periasamy, A., Fluorescence Microscopy Study of Heterogeneity in Polymer-Supported Luminescence-Based Oxygen Sensors. *Microsc. Microanal.* **2000,** *6*, 551-561.

7.   Lee, J.; Brennan, M. B.; Wilton, R.; Rowland, C. E.; Rozhkova, E. A.; Forrester, S.; Hannah, D. C.; Carlson, J.; Shevchenko, E. V.; Schabaker, D. S.; Schaller, R. D., Fast, Ratiometric FRET from Quantum Dot Conjugated Stabilized Single Chain Variable Fragments for Quantitative Botulinum Neurotoxin Sensing. *Nano Lett.* **2015,** *15*, 7161-7167.

8.   Kemling, J. W.; Qavi, A. J.; Bailey, R. C.; Suslick, K. S., Nanostructured Substrates for Optical Sensing. *J. Phys. Chem. Lett.* **2011,** *2*, 2934-2944.

9.   Rood, J. A.; Henderson, K. W., Synthesis and Small Molecule Exchange Studies of a Magnesium Bisformate Metal-Organic Framework: An Experiment in Host-Guest Chemistry for the Undergraduate Laboratory. *J. Chem. Educ.* **2013,** *90*, 379-382.

10.   Chen, T.-H.; Popov, I.; Kaveevivitchai, W.; Miljanic, O., Metal-Organic Frameworks: Rise of the Ligands. *Chem. Mater.* **2014,** *26*, 4322-4325.

11.   Keskin, S.; Kizilel, S., Biomedical Applications of Metal Organic Frameworks. *Ind. Eng. Chem. Res.* **2011,** *50*, 1799-1812.

12.   Schutting, S.; Borisov, S.; Klimant, I., Diketo-Pyrrolo-Pyrrole Dyes as New Colorimetric and Fluorescent pH Indicators for Optical Carbon Dioxide Sensors. *Anal. Chem.* **2013,** *85*, 3271-3279.

13. Sharon, E.; Freeman, R.; Willner, I., CdSe/ZnS Quantum Dots-G-Quadruplex/Hemin Hybrids as Optical DNA Sensors and Aptasensors. *Anal. Chem.* **2010,** *82*, 7073-7077.

14. Lakowicz, J. R., Introduction to Fluorescence. In *Principles of Fluorescence Spectroscopy*, 3rd ed.; Springer: 2006.

15. Demas, J. N.; DeGraff, B. A., Design and Applications of Highly Luminescent Transition Metal Complexes. *Anal. Chem.* **1991,** *63*, 829-837.

16. Carlson, B.; Eichinger, B. E.; Kaminsky, W.; Phelan, G. D., Complexes of Osmium with the 2-[(Diphenylphosphanyl)-methyl]-pyridine Ligand. *J. Phys. Chem. C* **2008,** *112*, 7858-7865.

17. (a) Meyer, T.; Meyer, G. J.; Pfennig, B. W.; Schoonover, J. R.; Timpson, C. J.; Wall, J. F.; Kobusch, C.; Chen, X.; Peek, B. M., Molecular-Level Electron Transfer and Excited State Assemblies on Surfaces of Metal Oxides and Glass. *Inorg. Chem.* **1994,** *33*, 3952-3964; (b) Terpetschnig, E.; Szmacinski, H.; Lakowicz, J. R., Fluorescence Polarization Immunoassay of a High-Molecular-Weight Antigen Using a Long Wavelength-Absorbing and Laser Diode-Excitable Metal-Ligand Complex *Anal. Biochem.* **1996,** *240*, 54-59; (c) Farzad, F.; Thompson, D. W.; Kelly, C. A.; Meyer, G. J., Competitive Intermolecular Energy Transfer and Electron Injection at Sensitized Semiconductor Interfaces. *J. Am. Chem. Soc.* **1999,** *121*, 5577-5578; (d) Sauvé, G.; Cass, M. E.; Coia, G.; Doig, S. J.; Lauermann, I.; Pomykal, K. E.; Lewis, N. S., Dye Sensitization of Nanocrystalline Titanium Dioxide with Osmium and Ruthenium Polypyridyl

Complexes. *J. Phys. Chem. B* **2000,** *107*, 6821-6836; (e) Trammell, S.; Meyer, T., Kinetics of Absorbed Chromophore Exchange on Metal Oxide Electrodes. *Langmuir* **2003,** *19*, 6081-6087; (f) O'Connor, M.; Killard, A.; O'Kennedy, R.; Forster, R.; Smyth, M., Production and Characterization of a Polyclonal Antibody for Os(II) and Ru(II) Polypyridyl Complexes. *J. Inorg. Biochem.* **2006,** *100*, 1252-1259; (g) Shen, W.; Deng, H.; Teo, A. K. L.; Gao, Z., An Electrodeposited Redox Polymer-Laccase Composite Film for Highly Efficient Four-Electron Oxygen Reduction. *J. Power Sources* **2013,** *226*, 27-32.

18.   Janis, J.; Jakonen, M.; Oresmaa, L.; Hirva, P.; Laurila, E.; Vlasova, L.; Vainiotalo, P.; Haukka, M., Fragmentation Pathways of [$MX_2(CO)_2$(dcbpy)] (M = Ru, Os; X = Cl, Br, I; dcbpy = 2,2'-bipyridine-4,4'-dicarboxylic acid) Complexes. *Organometallics* **2010,** *29*, 1070-1078.

19.   Chu, W.-K.; Yiu, S.-M.; Ko, C.-C., Neutral Luminescent Bis(bipyridyl) Osmium (II) Complexes with Improved Phosphorescent Properties. *Organometallics* **2014,** *33*, 6771-6777.

20.   Fu, Y.; Habtemariam, A.; Pizarro, A. M.; van Rijt, S. H.; Healey, D. J.; Cooper, P. A.; Shnyder, S. D.; Clarkson, G. J.; Sadler, P. J., Organometallic Osmium Arene Complexes with Potent Cancer Cell Cytotoxicity. *J. Med. Chem.* **2010,** *53*, 8192-8196.

21.   Moore, S. A.; Frazier, S. M.; Sibbald, M. S.; DeGraff, B. A.; Demas, J. N., On the Causes of Altered Photophysics of Luminescent Metal Complexes Embedded in Polymer Hosts. *Langmuir* **2011,** *27*, 9567-9575.

22. Lakowicz, J. R., Principles of Fluorescence Anisotropy. In *Principles of Fluorescence Spectroscopy*, 3rd ed.; Springer: 2006.

23. Lakowicz, J. R., Solvent and Environmental Effects. In *Principles of Fluorescence Spectroscopy*, 3rd ed.; Springer: 2006.

24. Cui, Y.; Yue, Y.; Qian, G.; Chen, B., Luminescent Functional Metal-Organic Frameworks. *Chem. Rev.* **2012,** *112*, 1126-1162.

25. Barrett, S. M.; Wang, C.; Lin, W., Oxygen Sensing *via* Phosphorescence Quenching of Doped Metal-Organic Frameworks. *J. Mater. Chem* **2012,** *22*, 10329-10334.

26. Demas, J. N.; DeGraff, B. A.; Coleman, P. B., Oxygen Sensors Based on Luminescence Quenching. *Anal. Chem.* **1999,** *71*, 793A-800A.

27. Maza, W. A.; Morris, A. J., Photophysical Characterization of a Ruthenium (II) Tris(2,2'-bipyridine)-Doped Zirconium UiO-67 Metal-Organic Framework. *J. Phys. Chem. C* **2014,** *118*, 8803-8817.

28. Bowman, R. D.; Kneas, K. A.; Demas, J. N.; Periasamy, A., Conventional, Confocal, and Two-Photon Fluorescence Microscopy Investigations of Polymer-Supported Oxygen Sensors. *J. Microsc.* **2003,** *211*, 112-120.

29. van Slageren, J.; Stufkens, D. J., Tuning the Excited-State Properties of [M(SnR$_3$)$_2$(CO)$_2$(a-diimine)] (M = Ru, Os; R = Me, Ph). *Inorg. Chem.* **2001,** *40*, 277-285.

30. Montalti, M.; Credi, A.; Prodi, L.; Gandolfi, M. T., *Handbook of Photochemistry*. 3rd ed.; CRC Press: 2006.
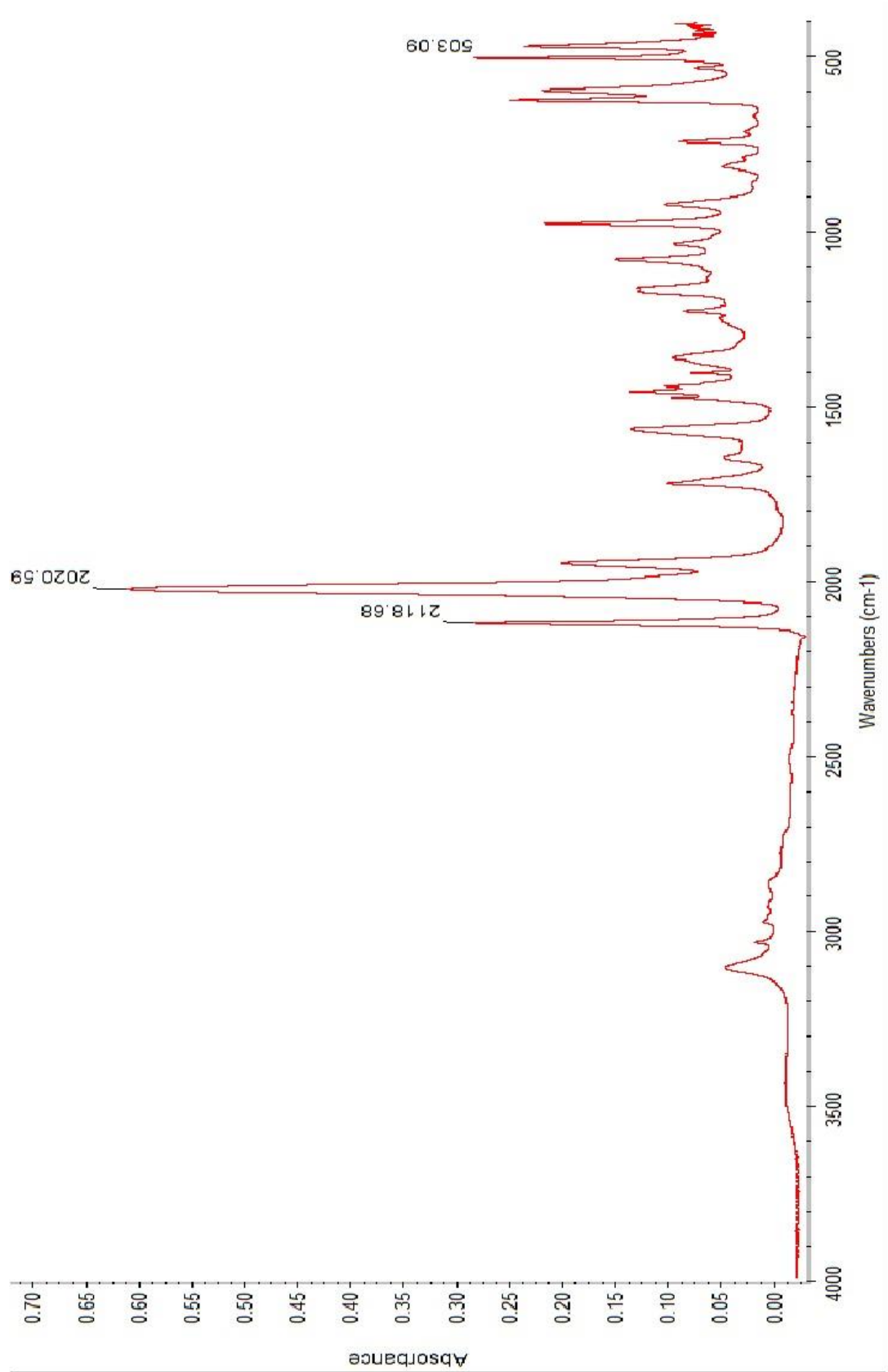
31.   Nozaki, K.; Takamori, K.; Nakatsugawa, Y.; Ohno, T., Theoretical Studies of
        Phosphorescence Spectra of Tris(2,2'-bipyridine) Transition Metal Compounds.
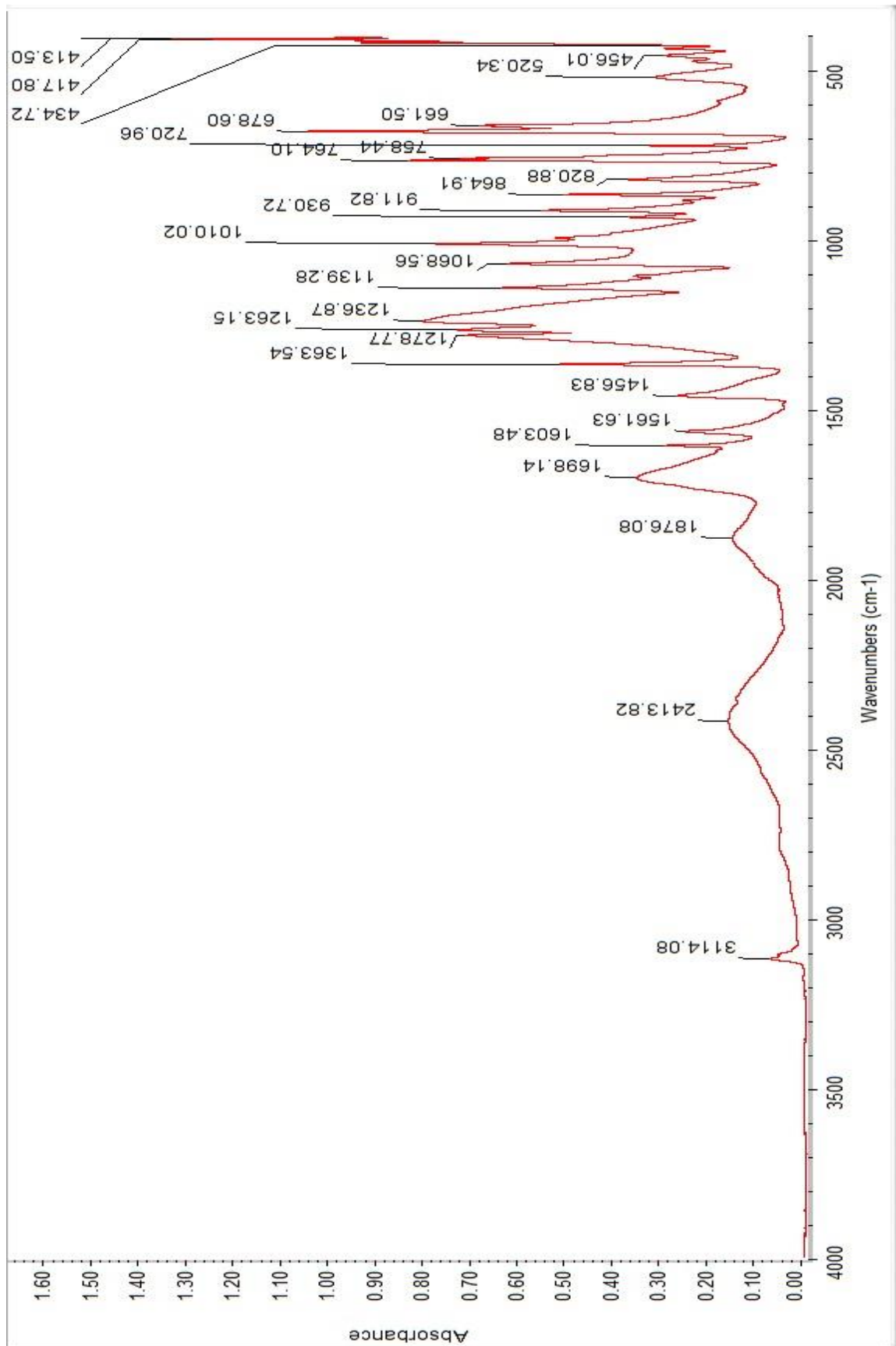   *Inorg. Chem.* **2006,** *45*, 6161-6178.
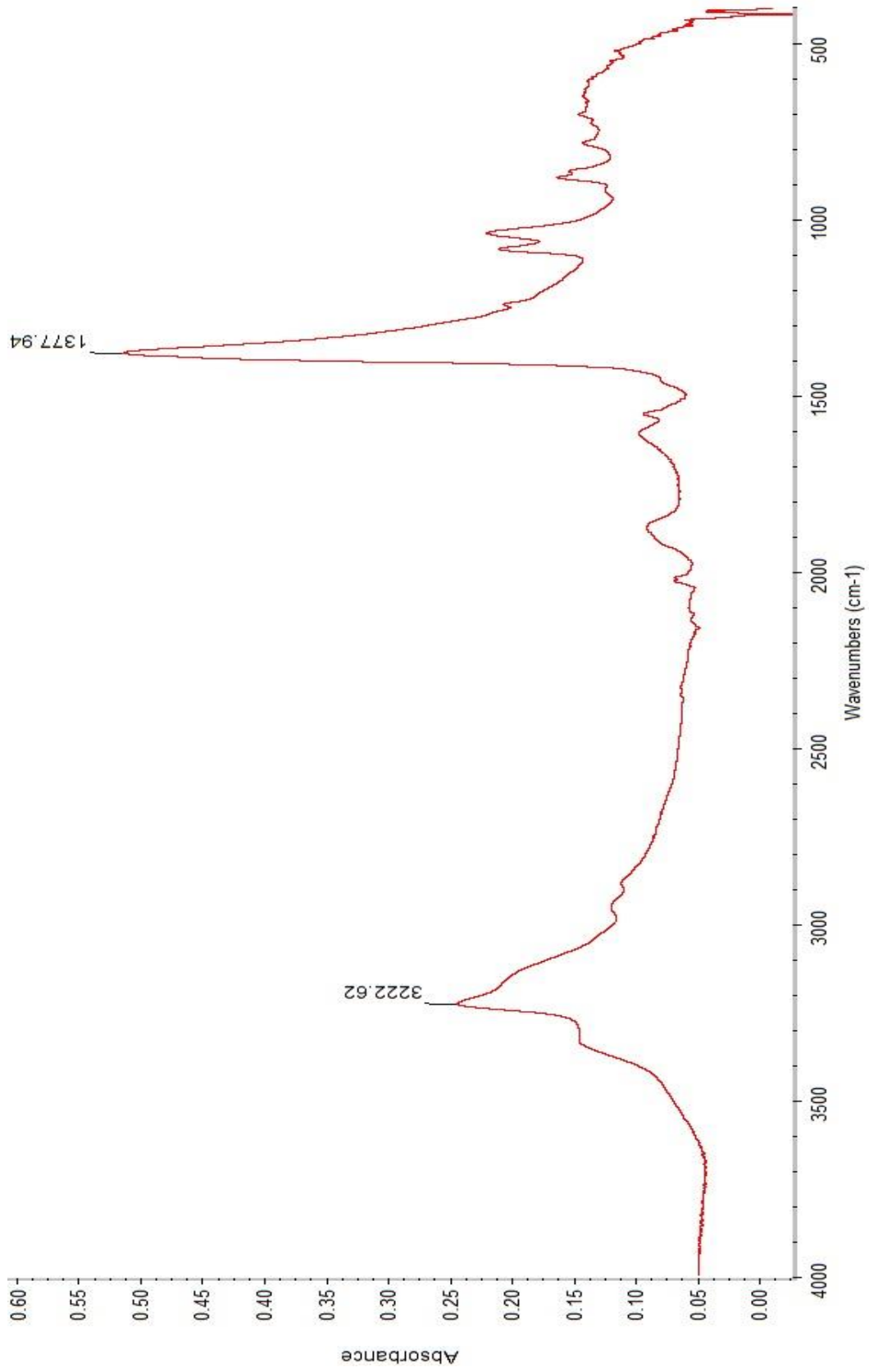
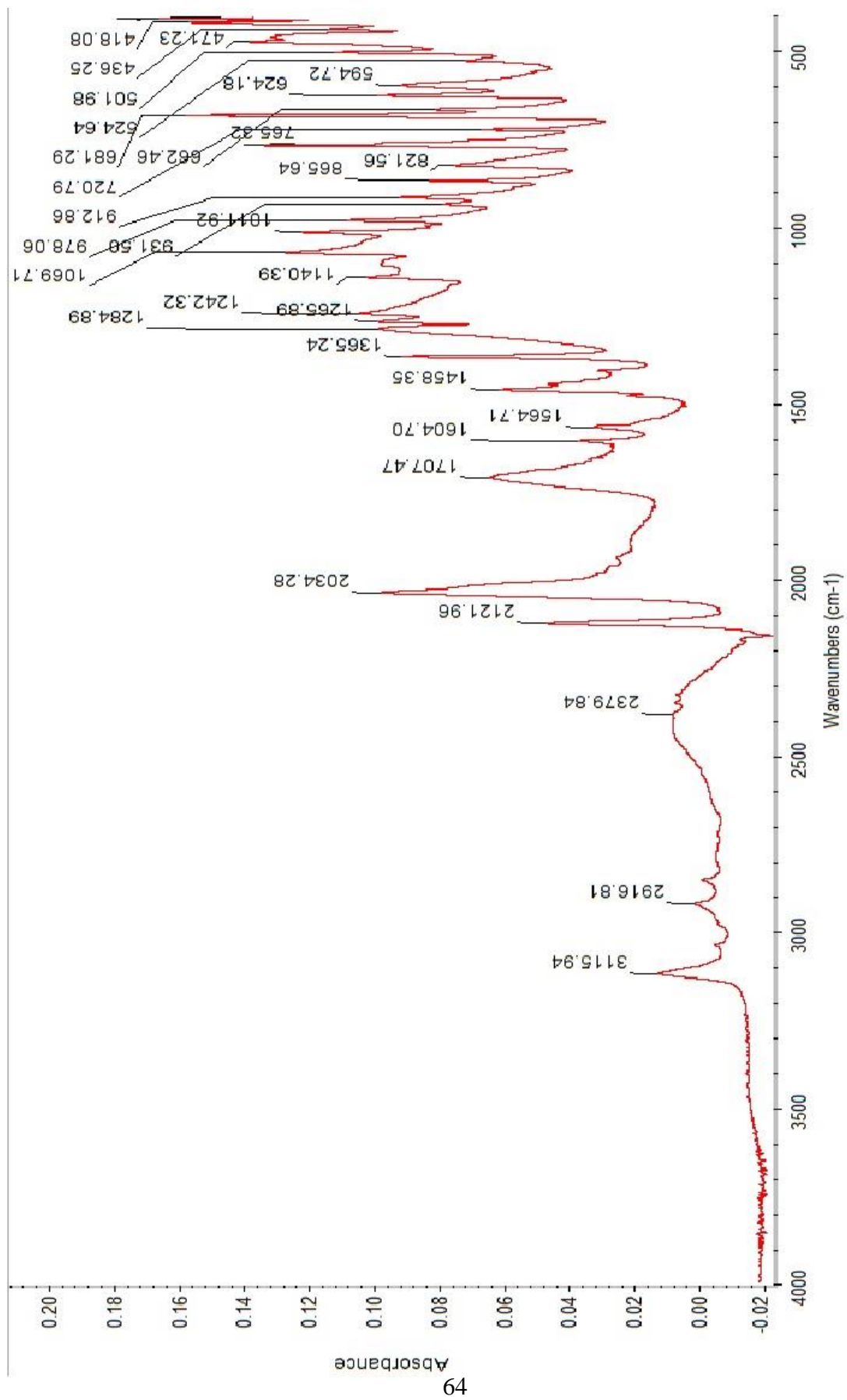**Appendix 1.** IR Spectrum of $(NH_4)_2OsCl_6$ Using the ATR Element
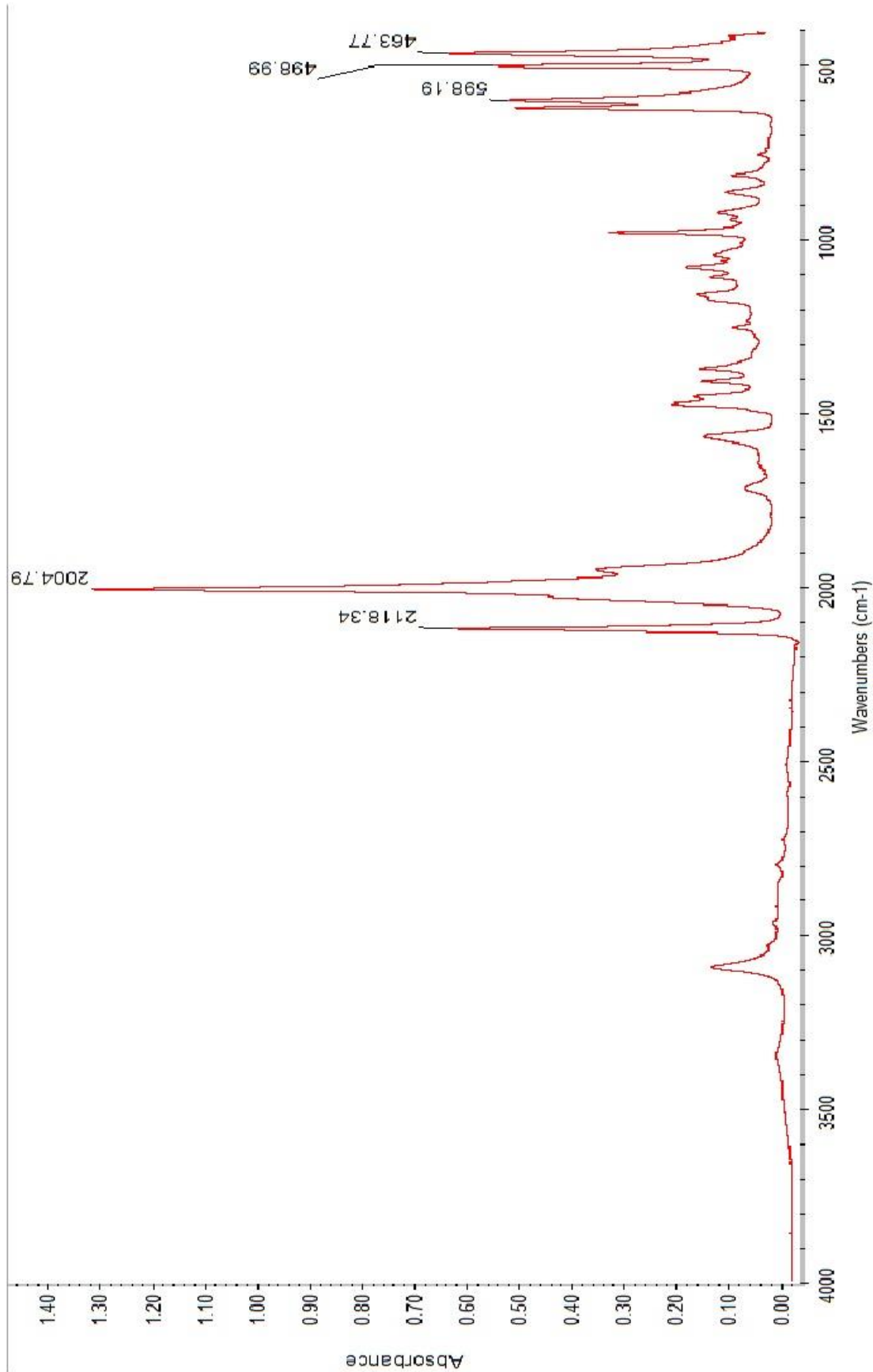
Appendix 2. IR Spectrum of Unpurified [Os(CO)$_2$Cl$_2$]$^{2+}$ Using the ATR Element

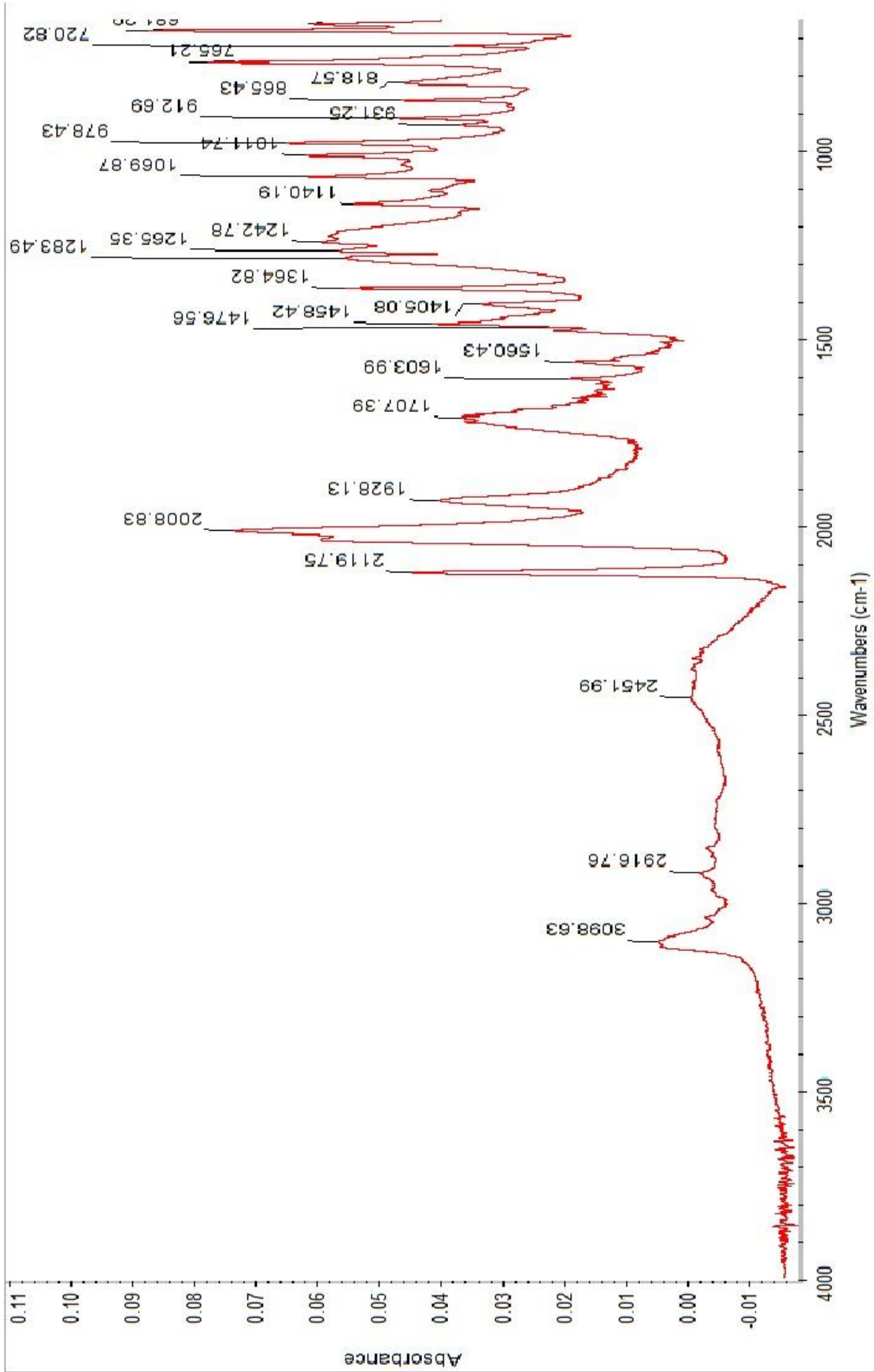**Appendix 3.** IR Spectrum of Recrystallized $[Os(CO)_2Cl_2]^{2+}$ Using the ATR Element

Appendix 4. IR Spectrum of of 2,2'-bipyridine-4,4'-dicarboxylic acid (dcbpy) Using the ATR Element

Appendix 5. IR Spectrum of $Os(CO)_2Cl_2(dcbpy)$ Using the ATR Element

Appendix 6. IR Spectrum of recrystallized Os(CO)$_2$Cl$_2$(dcbpy)] Using the ATR Element